

Stony Brook University



OFFICIAL COPY

The official electronic file of this thesis or dissertation is maintained by the University Libraries on behalf of The Graduate School at Stony Brook University.

© All Rights Reserved by Author.

Rheology and Structure of Thermoreversible Hydrogels

A Dissertation Presented

by

Jun Jiang

to

The Graduate School

in partial fulfillment of the

Requirements

for the Degree of

Doctor of Philosophy

in

Materials Science and Engineering

Stony Brook University

August 2007

Stony Brook University

The Graduate School

Jun Jiang

We, the dissertation committee for the above candidate for the

Doctor of Philosophy degree, hereby recommend

acceptance of this dissertation.

Dr. Miriam Rafailovich, Advisor
Department of Materials Science and Engineering

Dr. Jonathan C. Sokolov
Department of Materials Science and Engineering

Dr. Benjamin Chu
Department of Chemistry

Dr. Ralph H. Colby
Department of Materials Science and Engineering
Pennsylvania State University, University Park, PA

This dissertation is accepted by the Graduate School

Lawrence Martin
Dean of the Graduate School

Abstract of the Dissertation

Rheology and Structure of Thermoreversible Hydrogels

by

Jun Jiang

in

Doctor of Philosophy

Materials Science and Engineering

Stony Brook University

2007

Highly concentrated solutions of non-ionic amphiphilic triblock copolymer poly(ethylene oxide)₉₉-poly(propylene oxide)₆₇-poly(ethylene oxide)₉₉ (Pluronic F127) are widely used in numerous biomedical applications, such as drug delivery vehicles, and surfactants for emulsification of food and personal care products. The Pluronic copolymers are popular for these applications, since their gelation properties are thermoreversible and easily controlled by varying the concentration. They are liquid below room temperature and gel at body temperature. Hence they are great injectable biomaterials for tissue engineering and implantation.

In this dissertation, thermal gelation and structure of high concentration triblock copolymer Pluronic F127-clay (Cloisite Na⁺ and Lucentite SWN) aqueous solutions were characterized by rheological measurements, differential

scanning calorimetry (DSC) and small angle X-ray/neutron scattering. Small angle neutron scattering (SANS), under shear using a Couette cell in radial and tangential scattering geometry, was performed to examine the structural evolution of the polymeric micellar macro-lattice formed by concentrated aqueous solutions of triblock copolymer-Pluronic F127, as a function of the shear rate. The micellar gel showed a shear thinning, i.e., a reduction of the resistance to shear, by forming a layered stacking of two-dimensional hexagonally close packed (HCP) polymer micelles. A theoretical model was developed to calculate 2D SANS scattering patterns that can be compared with the experimental data.

In order to improve the mechanical properties of the gel, while still maintaining the thermo-reversibility, we synthesized multiblock structures, where the F127 construct would be repeated several times. In this manner, physical interconnections between the micelles could occur as the multiblock copolymers formed interlocking loops and tails, thereby greatly increasing the mechanical strength of the gels. The rheological and structural properties of the gels were characterized as a function of temperature, composition and degree of polymerization. For F127 solutions just below their gel point, substitution of F127 with as little as 1% multiblock succeeded in forming a physical gel. Percolation theory was used to understand the modulus growth when multiblock was added to F127 solutions just below their gel point, assuming the multiblocks form bridges between adjacent micelles.

To My Family

Table of Contents

Abstract.....	iii
List of Figures.....	viii
List of Tables.....	xiii
Acknowledgement.....	xiv
Chapter 1 Introduction	
1.1 Overview of Rheology and Structure of Hydrogels.....	1
1.2 Motivation of the Work.....	5
1.3 Outline of Chapters.....	6
1.4 References.....	9
Chapter 2 Rheological and Structural Characterization of Pluronic Polymer	
Hydrogels with added Salts or Clays	
2.1 Introduction.....	12
2.2 Experimental Section.....	14
2.3 Results and Discussion.....	18
2.4 Conclusions.....	23
2.5 References.....	25
Tables/Figures.....	27

Chapter 3 Shear Induced Layered Structure of Polymeric Micelles by SANS	
3.1 Introduction.....	42
3.2 Experimental Section.....	46
3.3 Results and Discussion.....	53
3.4 Conclusions.....	56
3.5 References.....	58
Figures.....	60
 Chapter 4 Rheology of Thermoreversible Hydrogels from Multiblock Associating Polymers	
4.1 Introduction.....	68
4.2 Experimental Section.....	70
4.3 Results.....	72
4.4 Discussion.....	78
4.6 Conclusion.....	80
4.7 References.....	81
Tables/Figures.....	83

List of Figures

Figure 2.1	DSC-measurements on the different concentration solutions of Pluronic F127.....	29
Figure 2.2	Micellization temperature as a function of the Pluronic F127 concentration.....	30
Figure 2.3(a)	DSC-measurements on 25% F127 with CNa clay.....	31
Figure 2.3(b)	DSC-measurements on 25% F127 with CaCl ₂ and NaCl salts.....	32
Figure 2.4	SAXS intensity profile of 30 wt % F127 in H ₂ O. The arrows indicate the peak positions. The numbers represent the ratio of the peak position relative to the first order peak.....	33
Figure 2.5	SANS intensity patterns of (a) 30 wt % F127 in D ₂ O; (b) 30 wt % F127 with 1 wt % NaCl in D ₂ O; (c) 30 wt % F127 with 2 wt % added bovine serum albumin in phosphate buffered saline (PBS).....	34
Figure 2.6	Elastic modulus as a function of strain for gels with 30 wt % Pluronic F127 with and without Cloisite Na ⁺ (CNa) clay. The oscillating frequency is 1 rad/s and temperature is 37 °C.....	35
Figure 2.7	Storage modulus of 30% F127 during heating at 1°C/min, with and without Cloisite Na ⁺ clay at a frequency of 1 rad/s and strain of 0.001.....	36

Figure 2.8	Storage modulus of 30% F127 during heating at 1°C/min, with and without SWN clay at a frequency of 1 rad/s and strain of 0.001.....	37
Figure 2.9	Storage modulus of 30% F127 during heating at 1°C/min, with and without NaCl at a frequency of 1 rad/s and strain of 0.001.....	38
Figure 2.10	Storage modulus of 30% F127 during heating at 1°C/min, with and without CaCl ₂ at a frequency of 1 rad/s and strain of 0.001.....	39
Figure 2.11	Elastic modulus of the gel as a function of the additive concentration.....	40
Figure 2.12	The sol-gel transition temperature as a function of the additive concentration.....	41
Figure 3.1	Schematic representations of Pluronic F127 micelles: (a) single micelle with spherical core-shell geometry; (b) single 2D hexagonally packed layer of micelles; (c) two 2D hexagonally packed layers of micelles (AB); and (d) three layers with ABC (or FCC) stacking sequence structure. Figures (b–d) correspond to the radial geometry.....	60
Figure 3.2	Tangential views of (a) ABC stacking sequence or FCC structure; (b) ABA stacking sequence or 3D hexagonal structure; and (c) Random AB stacking sequence.....	61

Figure 3.3	Configuration of the Couette cylinder used for the SANS measurements.....	62
Figure 3.4	Steady shear viscosity η , as a function of the shear rate $\dot{\gamma}$, on a micelle gel of 20% Pluronic F127 in D ₂ O.....	63
Figure 3.5	SANS radial scattering patterns from a to i for a 20% Pluronic F127 gel as a function of the shear rate: 0, 0.01, 1, 5, 10, 15, 30, 50 and 600 1/s.....	64
Figure 3.6	Calculated radial scattering patterns from a to i for a 20% Pluronic F127 gel, adapted for the experimental SANS patterns of Figure 3.5.....	65
Figure 3.7	SANS tangential scattering patterns from a to i for a 20% Pluronic F127 gel as a function of the shear rate: 0, 0.01, 1, 5, 10, 15, 30, 50 and 600 1/s	66
Figure 3.8	Calculated tangential scattering patterns from a to i for a 20% Pluronic F127 gel, adapted for the experimental SANS patterns of Figure 3.7.....	67
Figure 4.1	Chain extension of Pluronic F127 with hexamethylene diisocyanate.....	84
Figure 4.2	DSC measurements on the 20% solutions of different multiblock copolymer at 1 °C/min heating rate.....	85

Figure 4.3	SANS scattering profiles of different PF copolymer gels at 37 °C at rest.....	86
Figure 4.4	SANS scattering patterns for: (a) 20% F127 gel; (b) 20% PF 4.6 gel; and (c) Mixture of 18% F127 and 2% PF 4.6, with increasing the shear rate 0, 1, 10 and 100 1/s. Shear direction is perpendicular to the beam direction.....	87
Figure 4.5	Frequency dependence of storage and loss modulus of 20% PF 3.2 and 20% F127 (inset) at a strain of 0.001 and 37 °C.....	88
Figure 4.6	Storage modulus as a function of strain amplitude for 20% gels of F127 and different PF multiblock copolymers at a frequency 1 rad/s and 37 °C.....	89
Figure 4.7	Storage modulus of different concentrations of PF 3.2 polymer gels during heating at 1 °C/min at a frequency of 1 rad/s and strain amplitude of 0.001.....	90
Figure 4.8	Storage modulus and gelation temperature (inset) of PF 3.2 gels as functions of concentration.....	91
Figure 4.9	Storage modulus of 20% polymer gels during heating at 1 °C/min at a frequency of 1 rad/s and strain amplitude of 0.001.....	92
Figure 4.10	Storage modulus of 20% polymer gels as a function of degree of polymerization.....	93

Figure 4.11	Storage modulus of 25% polymer gels of F127/PF 4.6 mixtures as a function of the concentration of PF multiblock copolymer.....	94
Figure 4.12	Storage modulus of F127 and F127/PF 4.6 mixtures, all with an overall concentration of 14.5%, during heating at 1 °C/min at a frequency of 1 rad/s and strain amplitude of 0.001. (The inset represents of the storage modulus of low PF 4.6 concentrations which is not distinguishable in the scale of original figure.).....	95
Figure 4.13	Maximum value of the (high temperature) storage modulus of gels made by mixing F127 with three different multiblocks, all with an overall concentration of 14.5%, as a function of the concentration of PF multiblock copolymers. Equation 1 suggests that this plot should yield a straight line that extrapolates to c_{gel} at $G = 0$	96
Figure 4.14	Schematic diagram for intermicellar interaction with corresponding observations in scattering and rheology measurements: (a) F127 triblock copolymer; (b) mixture of F127 and PF multiblock copolymers.....	97

List of Tables

Table 2.1	The elastic modulus (37 °C) and sol-gel transition temperature for the Pluronic F127-Clay gels.....	27
Table 2.2	The elastic modulus (37 °C) and sol-gel transition temperature for the Pluronic F127-Salt gels.....	28
Table 4.1	Molecular Characteristics of Triblock F127 and the Multiblock Copolymers.....	83

Acknowledgement

There are many people I would like to thank for their support and encouragement. Without their generous help, mentally and physically, this dissertation would not have been possible.

First of all, I would like to thank my advisors, Professor Miriam Rafailovich and Professor Jonathan Sokolov for their constant guidance and leadership. It is you who bring me here, provide me all the learning opportunity and give me this great training. You are great mentors as well as great friends. Without your foresight, I may never have started down the path that I have taken.

To Professor Ralph Colby and Professor Ben Chu, thank you for being my committee members for my prelims and now for my dissertation. Thank you for your insightful discussions and suggestions, which greatly speed up the progress of my projects.

To Dr. Min Y. Lin, Dr. Christrain Burger, Dr. Jun Li, and Jack Lambardi, thank you for the collaboration on Neutron Scattering experiments and theory, and rheology. Without your friendship and support, I would have overcome so many barriers.

To my colleagues: Dr. Xuesong Hu, Dr. Haobin Luo, Dr. Wentao Li, Dr. Vladimir Zaitsev, Dr. Valadimir Samuilov, Dr. Yantian Wang, Dr. Mayu Si, Dr. E Guan, Dr. Clive. Li, Dr. Harry Xavier, Dr. John Jerome, Dr. Radha Ramasamy,

Dr. Xiaohua Fang, Dr. Bingquan Li, Dr. Yuan Ji, Yuan Sun, Zhi Pan, Charlie Chou, Xiaolan Ba, Sijia Zhao, Ying Liu, Ja Seung Koo, Wilson Lee, Seongchan Pack, Minhua Shao and Karthik Subburaman, thank you for making the workplace comfortable and enjoyable and thank you for always being there whenever I need your help.

My special thank you goes to my uncle in Law, Jason Li, and his family: my aunt, Haxia Zu, my cousins, Cheryl Li and Christine Li. They make me feel at home during this oversea study. Uncle Jason is my life mentor, from sports to career, from technical to personal. You are the person who makes me stronger.

To my parents, Yanqing Jiang and Surong Zhang, this thesis is for you. You work so hard to support my education. You believe in education and always encourage me to pursue my goals and dreams. Thank you for your support, encouragement and love. I'd also like to thank my parents in law, Zhiping Li and Yuzhi Wu, thank you for constant support and encourage.

Last but not the least, to my beautiful and lovely wife, Chunhua Li. You inspired my life. You are the best gift that I've ever received in my life. On the road of our Ph.D journey, we have traveled, argued, laughed,I cherish every moment we spent together on this road– the loneliness of doing experiments in the long hours, the thrill of the first publication, and the disappointment of the job searching. It is you who made this journey special and meaningful to me. Thank you for everything. I love you.

CHAPTER 1

Introduction

1.1 Overview of Rheology and Structure of Thermoreversible Hydrogels

Thermoreversible hydrogels attract lively research interest, despite their millennia-long history of use as food components [1-3]. The most seemingly obvious feature of thermoreversible hydrogels is their ability to gel, i.e., to transition, in a certain temperature region, from a viscous liquid to an assembly of effectively infinite-molecular weight physically cross-linked molecules with significant elasticity. Due to their thermoreversible gelation property, concentrated solutions of non-ionic amphiphilic triblock copolymers like poly(ethylene oxide)_x-poly(propylene oxide)_y-poly(ethylene oxide)_x (PEO_x-PPO_y-PEO_x, Pluronic) are being widely used in numerous biomedical applications, such as drug delivery, gels for replacing biological fluids such as synovial fluid and nucleus pulposus, and surfactants for emulsification of food and personal care products [4,5]. Numerous studies have been performed using a battery of complementary techniques [6-9], to try to understand the structure-property relations responsible for the formation of these “smart” gels. The structure and

dynamics of micellization, and phase diagrams and aggregation behavior of Pluronic polymer gels have been reported by several groups, Mortensen, Alexander and Wanka *et al* [10-12]. At low polymer concentrations, light scattering measurements corroborate the aggregation of copolymers into spherical micelles and allow the determination of the micelle size [6]. FTIR spectroscopy was used to investigate of effects of temperature and concentration on PEO-PPO-PEO block copolymer properties in aqueous solutions [13]. Guo *et al* studied the micellar structure changes in aqueous mixtures of nonionic surfactants and PEO-PPO-PEO triblocks[14].

Combining small angle X-ray scattering (SAXS) and small angle neutron scattering (SANS), Wu *et al* have shown that at high concentrations the micelles organized into a face centered cubic structure [6]. Prud'homme *et al* proposed is that the ordered micelle structures are due to repulsive interactions among close-packed spherical micelles [7], and hence the material was a “micelle gel” as opposed to a chemical gel where the components are linked by covalent bonds. Morphology of these gels has been characterized by AFM and Cryo-TEM [8,9].

The rheological and gelation properties of Pluronic polymer solutions can be affected by the presence of various additives. The effects of the additives, such as salt, ionic surfactants, and drug molecules, on phase behaviors of the dilute polymer solutions have been studied [15-18]. A series of investigations showed that the presence of salting-out electrolytes, such as NaCl, NaF would decrease

both critical micellization concentration (CMC) and critical micellization temperature (CMT) values, whereas salting in electrolytes like NaI, NaNCS and non-electrolytes such as small chain alcohols, urea, have opposite effect [16]. The PEO-PPO-PEO triblock co-polymers are known to interact with ionic surfactants [17,18], which are often used in the processing of various triblock copolymer formulations in several industries.

The organization of micelles into layers adapted to laminar shear flow is responsible for the exceptional visco-elastic properties of these systems, especially when being subjected to shear forces. Consequently, the structure-property relationships are dynamic and vary with the shear rate. Hence, it is important to understand their correlation with rheology as a function of the shear rate. Since the pioneering work of Hoffman, Ackerson and Loose [19-21] on shear-induced transitions in suspensions of charged particles, much effort has been made to identify the structural properties of colloidal crystals under shear. More recently [22, 23], it has been shown that the selective solvent properties of diblock or triblock copolyethers like polyethylene oxide (PEO), polypropylene oxide (PPO) or polybutylene oxide (PBO) in aqueous solution can lead to the formation of micelles with a spherical core-shell geometry. While dilute solutions contain discrete micelles, concentrated solutions can form highly ordered arrangements of micelles, characterized by a certain overlap of the coronae of neighboring micelles. Especially in a shear environment, the packing order is

dominated by 2D hexagonally packed layers of micelles. The oriented structures of several similar copolymers under steady shear have been studied by SANS and SAXS [24-29]. For instance, using scattering techniques on both tangential and radial geometry, Molino, Diat and Slawacki *et al* [24-27], showed the shear orientation effects on the micelle system of Pluronic F85 and F108. The structure and flow behavior of block copolymers has been reviewed by Ian W Hamley [29]. In Chapter 3, we present several extensions to the theoretical scattering analysis by Loose and Ackerson [20,21] on which all previous data evaluation was based, and apply it to experimental SANS data under shear for the F127 copolymer system.

On the other hand, the lack of chemical cross-links results in the F127 micelle gel having a very low yield strength as the micelle layers can easily slide past each other under shear [30]. Hence, the rheological and structural properties of F127 gels limit its applications in some fields, such as tissue engineering and implantation, which requires high elastic modulus and yield strain. The chemical crosslinkable gels have been studied, by Cohn *et al* [31], to improve the mechanical properties of gels. The dynamics and elasticity of polymer network has been studied by Rubinstein and Semenov [32,33]. In Chapter 4, we make use of these ideas to understand the effects of adding small quantities of Cohn's chain extended multiblock copolymers to F127 solutions.

1.2 Motivation of the Work

Despite the frequent uses of these gels in pharmaceuticals and medicine, only a few studies [34,35] exist which have measured their properties at high concentration and under physiological conditions and with added clays. Therefore, in this work, we investigated the effects of the salts and clays on the rheological and structural properties of highly concentrated copolymer solutions.

The traditional Couette scattering geometry with the neutron beam centered at the Couette cell (“radial” geometry) corresponds to the perpendicular situation of Figure 1d, so that most information about the stacking sequence is lost in the projection onto the plane normal to the beam. In order to extract the stacking sequence information, an experiment in “tangential” geometry needs to be performed.

Due to the lack of actual cross-links, the F127 micelle gels have very low yield strength. In order to improve the mechanical properties of the gel, while still maintaining the thermo-reversibility, we synthesized multiblock structures, where the F127 construct would be repeated several times. In this manner, physical interconnections between the micelles could occur as the multiblock copolymers formed interlocking loops and tails, thereby greatly increasing the mechanical strength of the gels. Furthermore, by adding even a small amount of the multiblock to the F127 gels, we propose a model where a large enhancement of the mechanical properties could occur, as the longer chains could span more than

one micelle. This allows a new class of thermoreversible gels to be made where the rheological properties can be tailored to specific applications.

1.3 Outline of Chapters

In chapter 2, we have characterized the thermal gelation and structure of high concentration triblock copolymer (Pluronic F127)-clay (Cloisite Na⁺ and Lucentite SWN) aqueous solutions by using rheological measurements, differential scanning calorimetry (DSC) and small angle X-ray/neutron scattering. The sol-gel transition temperature, as well as the elastic modulus of the F127 solution depends both on the concentration of polymer and of clay. Above the gel transition, the elastic modulus of the solutions increased with clay concentration. Yield strain is independent of polymer and clay concentrations. Two different kinds of inorganic salts, sodium chloride (NaCl) and calcium chloride (CaCl₂) were added into the polymer and polymer-clay solutions. We found that, the sol-gel transition temperature and elastic modulus of these systems decreased only a small amount with increasing concentration of inorganic salts. Addition of salts to polymer clay solutions resulted in precipitation of the clays which decreased the modulus. In each case the scattering patterns corresponded to one large oriented macro-domain at zero shear with a distance of 19.2 nm between two close packed micelles.

In chapter 3, small angle neutron scattering (SANS), under shear using a Couette cell in radial and tangential scattering geometry, was performed to examine the structural evolution of the polymeric micellar macro-lattice formed by concentrated aqueous solutions of F127, as a function of the shear rate. The micellar gel showed a shear thinning, i.e., a reduction of the resistance to shear, by forming a layered stacking of two-dimensional hexagonally close packed (HCP) polymer micelles. While traditional SANS experiments using a Couette shear cell are performed in radial geometry, we found the use of the tangential scattering geometry essential to obtain information on the layer stacking sequence. A theoretical model was developed to calculate 2D SANS scattering patterns that can be compared with the experimental data. We found that the micellar cores maintained their spherical shapes without deforming into ellipsoids, and that the intra-layer neighboring micelle center-to-center distance and the inter-layer long period were independent of the shear rate and only depended on the concentration of the polymer. We also found that the stacking sequence changed from asymmetrically twinned ABC (i.e., FCC) at low shear rates to random AB stacking at high shear rates.

In chapter 4, multiblock copolymers of F127 were synthesized by chain extending with hexamethylene diisocyanate (HDI). The resulting multiblock copolymer poly-F127 maintained the thermoreversible properties of the original F127 triblock unit. The rheological and structural properties of the gels were

characterized as a function of temperature, composition and degree of polymerization. Neutron scattering reveals a large degree of alignment could be induced in the F127 gel, but no long-range order could be found in the multiblocks or the mixtures of F127 with multiblocks. The shear strain at yield in polymers having an average of 3.2 or more F127 repeats was nearly an order of magnitude higher than the F127 gel. Consequently, control of both F127 concentration and multiblock concentration allows gel modulus and yield strain to be independently tuned. For F127 solutions just below their gel point, substitution of F127 with as little as 1% multiblock succeeded in forming a physical gel. Percolation theory was used to understand the modulus growth when multiblock was added to F127 solutions just below their gel point, assuming the multiblocks form bridges between adjacent micelles.

1.4 References

- [1] Xiong, X. Y.; Tam, K. C.; Gan, L. H. *Journal of Nanoscience and Nanotechnology* **2006**, 6, 2638–2650.
- [2] Chun, K. W.; Lee, J. B.; Kim, S. H. *et al. Biomaterials* **2005**, 26, 3319–3326.
- [3] Higuchi, A.; Yamamoto, T.; Sugiyama, K.; Hayashi, S.; Tak, T. M.; Nakagawa, T. *Biomacromolecules* **2005**, 6, 691–696.
- [4] Cohn, D.; Sosnik, A.; Garty, S. *Biomacromolecules* **2005**, 6, 1168–1175.
- [5] Matthew, J. E.; Nazario, Y. L.; Roberts, S. C.; Bhatia S. R. *Biomaterials* **2002**, 23, 4615–4619.
- [6] Wu, C.; Liu, T.; Chu, B.; Schneider, K. D.; Graziano, V. *Macromolecules* **1997**, 30, 4574–4583.
- [7] Prud'homme, R. K.; Wu, G.; Schneider D. K. *Langmuir* **1996**, 12, 4651–4659.
- [8] Wu, C.; Liu, T.; White, H.; Chu, B. *Langmuir* **2000**, 16, 656–661.
- [9] Mortensen, K.; Talmon, Y. *Macromolecules* **1995**, 28, 8829–8834.
- [10] Mortensen, K.; Pedersen, J. S. *Macromolecules* **1993**, 26, 805–812.
- [11] Alexandridis, P.; Holzwarth, J. F.; Hatton, T. A. *Macromolecules* **1994**, 27, 2414–2425.
- [12] Wanka, G.; Hoffmann, H.; Ulbricht, W. *Macromolecules* **1994**, 27, 4145–4159.
- [13] Su, Y.; Wang, J.; Liu, H. *Macromolecules* **2002**, 35, 6426–6431.
- [14] Liang Guo. PH.D Thesis, The Pennsylvania State University. **2003**

- [15] Jorgensen, E. B.; Hvidt, S.; Brown, W.; Schillin, K. *Macromolecules* **1997**, 30, 2355–2364.
- [16] Pandit, N.; Trygstad, T.; Croy, S.; Bohorquez, M.; Koch, C. *Journal of Colloid and Interface Science* **2000**, 222, 213–220.
- [17] Mata, J.; Joshi, T.; Varade, D.; Ghosh, G.; Bahadur, P. *Colloids and Surfaces A* **2004**, 257, 1–7.
- [18] Jansson, J.; Schillen, K.; Nilsson, M.; Söderman, O.; Fritz, G.; Bergmann, A.; Glatter, O. *Journal of Physical Chemistry B* **2005**, 109, 7073–7083.
- [19] Hoffman, R. L. *Trans. Soc. Rheol.* **1972**, 16, 155–173.
- [20] Ackerson, B. J.; Clark, N. A. *Phys. Rev. Lett.* **1981**, 46, 123–126.
- [21] Loose, W.; Ackerson, B. J. *J. Chem. Phys.* **1994**, 101, 7211–7220.
- [22] Castelletto, V.; Hamley, I. W.; Holmqvist, P.; Rekasas, C.; Booth, C.; Grossmann, J. G. *Colloid. Polym. Sci.* **2001**, 279, 621–628.
- [23] Daniel, C.; Hamley, I. W.; Mingvanish, W.; Booth, C. *Macromolecules* **2000**, 33, 2163–2170.
- [24] Diat, O.; Porte, G.; Berret, J. -F. *Physical Review B* **1996**, 5, 14869–14872.
- [25] Berret, J.-F.; Molino, F. R.; Porte, G.; Diat, O.; Lindner, P. *J. Phys.: Condens. Matter* **1996**, 8, 9513–9517.
- [26] Molino, F. R.; Berret, J.-F.; Porte, G.; Diat, O.; Lindner, P. *Eur. Phys. J. B* **1998**, 3, 59–72.

- [27] Slawecki, T. M.; Glinka, C. J.; Hammouda, B. *Physical Review E* **1998**, 58, R4084–R4087.
- [28] McConnell, G. A.; Lin, M. Y.; Gast, A. P. *Macromolecules* **1995**, 28, 6754–6764.
- [29] Hamley, I. W. *J. Phys.: Condens. Matter* **2001**, 13, 643–671.
- [30] Jiang, J.; Burger, C.; Li, C.; Lin, M. Y.; Rafailovich, M. H.; Sokolov, J. C. *Macromolecules* **2007**, 40, 4016–4012.
- [31] Cohn, D. et al. *J. Biomater. Sci. Polymer Edn* **2003** 14, 227–239.
- [32] Rubinstein, M.; Semenov, A. N. *Macromolecules* **2002**, 35, 6670–6686.
- [33] Semenov, A. N.; Rubinstein, M. *Macromolecules* **2002**, 35, 4821–4837.
- [34] Ricci, E. J.; Bentley, M.; Farah, M.; Bretas, R.; Marchetti, J. M. *European Journal of Pharmaceutical Sciences* **2002**, 17, 161–167.
- [35] Sharma, P. K.; Matthew, J. E.; Bhatia, S. R. *Journal of Biomaterials Science-Polymer Edition* **2005**, 16, 1139–1151.

CHAPTER 2

Rheological and Structural Characterization of Pluronic Polymer Hydrogels with added Salts or Clays

2.1 Introduction

Highly concentrated solutions of non-ionic amphiphilic triblock copolymer poly(ethylene oxide)₉₉-poly(propylene oxide)₆₉-poly(ethylene oxide)₉₉ (PEO₉₉-PPO₆₉-PEO₉₉) are widely used in numerous biomedical applications, such as drug delivery vehicles, gels for replacing biological fluids such as synovial fluid and nucleus pulposus, and surfactants for emulsification of food and personal care products [1,2]. The Pluronic copolymers are popular for these applications, since their gelation properties are thermoreversible and easily controlled by varying the concentration. They are liquid below room temperature and gel at body temperature. Hence they are easily injected and once they fill the proper cavity they gel as they reach body temperature. Furthermore the range of moduli achieved is easily superimposed on that of soft body tissues.

Numerous studies have been performed using a battery of complementary techniques [3-8] to try to understand the structure of these gels. In general, the copolymer Pluronic F127 aqueous solution is in a unimer state at low temperatures and low polymer concentration since both blocks (PEO and PPO) are water soluble at low temperatures. Increasing the temperature causes the formation of spherical micelles with a core of mainly the hydrophobic PPO blocks and a water-swollen corona of PEO blocks [3-6]. Combining small angle X-ray scattering (SAXS) and small angle neutron scattering (SANS), Wu *et al* have shown that at high concentrations the micelles organized into a face centered cubic structure [7]. Prud'homme *et al* proposed is that the ordered micelle structures are due to repulsive interactions among close-packed spherical micelles [8], and hence the material was a “micelle gel” as opposed to a chemical gel where the components are linked by covalent bonds.

The rheological and gelation properties of Pluronic polymer solutions can be affected by the presence of various additives. The effects of the additives, such as salt, ionic surfactants, and drug molecules, on phase behaviors of the dilute polymer solutions have been studied [9-13]. A series of investigations showed that the presence of salting-out electrolytes, such as NaCl, NaF would decrease both critical micellization concentration (CMC) and critical micellization temperature (CMT) values, whereas salting in electrolytes like NaI, NaNCS and non-electrolytes such as small chain alcohols, urea, have opposite effect [11]. The

PEO-PPO-PEO triblock co-polymers are known to interact with ionic surfactants [12,13], which are often used in the processing of various triblock copolymer formulations in several industries.

In the physiological environment, where many applications of these polymers exist, there are numerous charged molecules as well. In addition to different salts, and occasionally clays which are added to further increase the modulus. Despite the frequent uses of these gels in pharmaceuticals and medicine, only a few studies [14,15] exist which have measured their properties at high concentration and under physiological conditions and with added clays. Therefore, in this work, we investigated the effects of the salts and clays on the rheological and structural properties of highly concentrated copolymer solutions.

2.2 Experimental Section

Materials. Pluronic F127 (12 600 Daltons, 70 % w/w PEO) was obtained from BASF (Mount Olive, NJ, USA) and used without any further purification. The deionized water used was treated with Millipore-Q water purification system. Cloisite[®] Na⁺ (CNa) was purchased from Southern Clay Products Inc. (Texas, USA). It is a natural hydrophilic mineral (Na⁺-montmorillonite), which possesses a 2-to-1 layered structure with a single octahedral aluminum layer located

between two layers of silicon tetrahedron, and has a nominal chemical formula of $[(Al_{1.67}Mg_{0.33})Si_4O_{10}(OH)_2]Na_{0.33}\cdot nH_2O$. Each layered sheet is about 10 Å thick with lateral dimensions of 0.4-1 µm. This yields a specific surface area of ca. 725 m²/g. Lucentite SWN clay (Lithium Magnesium Sodium Silicate) was purchased from KOBO Products, (New Jersey, USA). Lucentite SWN clay is synthesized by reacting magnesium silicates and alkali cations that have superior transparency, high brightness and constant quality. It has very low impurity content compared with natural clay. The inorganic salt Calcium Chloride (CaCl₂) was purchased from FisherChemicals (New Jersey, USA). The Sodium Chloride (NaCl) was purchased from J. T. Baker (New Jersey, USA).

Sample preparation. Gels were prepared on a weight basis using the cold method.¹⁶ Concentrations of Pluronic polymer F127 and clays are expressed by weight percentage (% w/w). Pluronic polymer was dissolved in de ionized (DI) water and stirred at 4 °C. The solution was then put into the refrigerator at 4 °C for 1-2 days until it gets clear. In order to obtain a polymer-clay solution, we first dissolved clay in DI-water while stirring for 24 hours. In order to further exfoliate the clay, the solution was subsequently sonicated for one hour. The DI-clay solution was placed into an ice bath and the F127 polymer was added. In order to ensure that the polymer was completely dissolved, the entire solution was then refrigerated at 4 °C.

S

Differential Scanning Calorimetry (DSC). A Mettler Toledo DSC 821e differential scanning calorimeter was used to study the heat capacity of solutions as a function of temperature between 2 and 50 °C. Typically 6-12 mg solutions were placed in aluminum pans, which were then carefully sealed. The scans were carried out in a dry nitrogen environment at a constant heating rate of 2 °C /min, with an empty aluminum pan as reference.

SAXS. SAXS experiments were performed at the X3A2 State University of New York (SUNY) beam line, National Synchrotron Light Source (NSLS) at Brookhaven National Laboratory (BNL), using a laser-aided prealigned pinhole collimator [17]. The incident beam wavelength (λ) was tuned at 0.154 nm. The sample-to-detector distance was 1.09 m. The experimental data were corrected for background scattering and sample transmission.

SANS. To measure the structure of the Pluronic F127 gels, SANS experiments were performed at the National Institute of Standards and Technology reactor division. Data were collected on an area sensitive detector at the NG3 (NIST/Exxon/U.Minn) SANS Beamline, with sample to detector distances of 2.90 m. The nominal wavelength of the neutrons was 6.00 Å with a dispersity $\Delta\lambda/\lambda$ of 0.10 and an average incident intensity of approximately 35,000 neutrons/s, the accessible range in q 0.0054 to 0.1366 Å⁻¹, and the magnitude of the scattering vector defined by $(4\pi/\lambda)\sin(\theta/2)$, where θ is the angle between incident and scattered beam. A small aperture of approximately 1 cm in diameter was placed

before the sample to limit the width of the diffraction spots. The samples were placed inside a sample holder designed for SANS experiments. The sample thickness was 1 mm. Samples were loaded carefully at 2 °C to minimize the shear effects, and then the temperature was increased to the test temperature where it was stabilized for 20 min.

Rheological Measurement. Rheological measurements of polymer gels were performed on a strain-controlled rheometer, Rheometrics Fluids Spectrometer II, using concentric cylinders, with an inner diameter of 16.5 mm, an outer diameter of 17.1 mm and 13.7 mm height. Temperature control was achieved using a fluid bath surrounding the outer cylinder. The concentric cylinder geometry was loaded with the polymer solutions at 2 °C, in order to ensure that they were in the liquid state. Temperature sweep measurements were performed at a constant heating rate of 1 °C/min. Low viscosity silicone oil was added to the surface of the sample to minimize evaporation of the solvent.

The instrument was used in the oscillatory mode, in which the outer cylinder is rotated sinusoidally at a given frequency. The frequency dependence of the complex modulus was determined between 0.01 and 100 rad/s. The sol-gel transition temperature of F127 gels was determined from an oscillatory shear temperature sweep at 1 rad/s. The sol-gel transition temperature was measured for all the gels, as the temperature at which G' was half of the value for the high-temperature gel [18].

2.3 Results and Discussion

Differential Scanning Calorimetry. DSC measurements were carried out on block copolymer solutions as a function of polymer concentration. In Figure 2.1, we see that there is a large endothermic peak is observed in all spectra and the position of the peak is concentration dependent. The origin of the DSC peak was assumed to be caused by desolvation of the PPO groups [6]. Desolvation is also responsible for rendering the PPO hydrophobic at higher temperatures and hence in the case of the block copolymer solutions, is also known for be responsible for formation of micelles where the core is PPO and the corona is composed of the hydrophilic PEO block. The peak is somewhat broad due to the fact that the copolymer we used has a relatively broad polydispersity of $M_w/M_n \sim 1.6$. Hence in Figure 2.2 we plot the position of the peak or the micellization temperature as a function of polymer concentration. From the figure we find that the micellization temperature (T_m) decreases linearly with increasing concentration, as expected [6] since the increased polymer concentration also decreases the entropy of micellization. It is interesting to note in Figure 1 that a small endothermic peak appears approximately five degrees above the micellization transition. This peak is only observed for concentrations greater than 15 % and corresponds to the formation of a micelle ordered phase from the isotropic micellar solution. The temperature at which the high temperature peak occurs is in good agreement with

the value determined from rheological measurements at which the storage modulus starts to grow rapidly.

In Figure 2.3 a, we show the DSC spectra obtained with the addition of CNa clay. The clay has no effect on the thermodynamic response of the gel. On the other hand in Figure 2.3 b, we show the data obtained when 1 % (NaCl and CaCl₂) salts are added to the polymer. We can see that the decrease of the micellization temperature can be significantly effected by the concentration of salts. From these data we can conclude that the presence of salt enhances the desolvation of the PO since Na⁺ may displace the water hydrogen bonded to the other oxygen on PO. Even though Ca²⁺ is a divalent ion, which was expected to affect micellization, the Na⁺ ions were more effective apparently because they are more active in desolvation. It is interesting to note that even though a significant amount of Na⁺ is present in clays (CNa and SWN) they do not affect the micellization temperature. This indicates that the Na⁺ is bound to the clay and does not displace water on the polymer. Furthermore, since the clay does not affect the yield strain, we suspect that only minimal interactions between the clay and the block copolymer exist.

SAXS and SANS: The effect of addition of clays and salts on the structure of the gels. Structural studies on Pluronic F127 gels were performed using SAXS and SANS. Figure 2.4 shows the SAXS intensity profile of 30 % F127 in H₂O, showing the usual ring structure already reported by Wu *et al* [7] On the basis of

the Bragg diffraction peaks from SAXS we are able to determine the F127 gel structure as a polycrystalline face-centered cubic (FCC) lattice. The corresponding diffraction planes can also be indexed as (111), (200), (220), (311) and (222), which were also consistent with SAXS data reported by Wu *et al.* In Figure 2.5 a and 2.5 b we show the SANS intensity patterns of 30 % F127 gel in D₂O and 30 % F127 gel with 1 % NaCl added in D₂O respectively. Compared with Figure 2.5 a, from Figure 2.5 b we can see that in this case a highly oriented crystalline pattern was found which means that the complete irradiated volume formed one crystalline-domain. The pattern can be interpreted in terms of a stacking of 2D hexagonally packed layers of micelles [19]. The layers of micelles were perpendicular to the beam. By fitting the positions of the diffraction peaks, we deduced that the micelles had a distance of 19.2 nm between two close packed micelles, which is similar with what was found for the polycrystalline gel without salt. Salts are known to reduce the solvent quality of water for both PEO and PPO. This should make the micelle core denser. Why this causes the formation of macroscopic crystals is not yet clear.

The effects of added salts and clays on the rheological properties. To measure the linear viscoelastic properties, it is necessary to determine the linear viscoelastic region. This region was determined by measuring the elastic modulus G' and the loss modulus G'' as a function of the strain amplitude, using a 30 % F127 gel. The strain amplitude sweep was measured between 0.0003 and 1 at 1

rad/s. From Figure 2.6, it was observed that G' and G'' are independent of strain amplitude up to 0.01. Therefore, a strain amplitude of 0.001 at 1 rad/s shear rate was used for all the dynamic measurements, in order to remain in the linear regime and preserve the internal structure.

In Figure 2.6, we also show that the CNa clay effects on the yield strain of the gels. The yield strain did not increase with increasing clay concentration, even though CNa clay is known as a viscosity modifier for water since it can exfoliate and form a gel.

The temperature dependence of rheological properties of the gels was studied at a range of 2 to 40 °C. In Figure 2.7, we plot the elastic modulus G' as a function of temperature. The elastic modulus is low at low temperature but it increases dramatically with increasing temperature as a result of the gel forming process. At the end of the sol-gel transition, G' plateaus becomes independent of the temperature. The effect of the clay concentration on the elastic modulus and the sol-gel transition temperature of the gels are shown in Figure 2.7 and Figure 2.8 for the systems with CNa and SWN clays, respectively. We find that the two clays behaved in a similar manner; the sol-gel transition temperature decreased and G' increased with the increasing concentration of both clays (see Table 2.1). Since both of CNa and SWN clays are hydrophilic, they are able to hydrogen bond with water molecules. It is known that when the clay concentration exceeds $\sim 2\%$ they are able to form a gel at temperatures as low as 4 °C due to charge-charge

interactions [21]. As can be seen from Figure 2.3 this gelation does not affect the micellization temperature of the polymer, as expected, since it does not interact very strongly with the polymers. The ordering of the clay platelets may confine the micelles and induce micelle ordering at a lower temperature, as illustrated in the cartoon in the inset of Figure 2.8. This will not affect the yield point since no additional entanglements between the micelles occurred. On the other hand, the presence of the clay provides resistance to the shear, hence effectively increasing the modulus of the solution.

The solubility, rheological properties and the gelation process of the Pluronic F127 in water can be changed in the presence of inorganic salts such as NaCl and CaCl₂. The elastic modulus as a function of temperature for the 30 % F127 gel with different concentrations of NaCl and CaCl₂ are shown in Figure 2.9 and Figure 2.10, respectively. We find that the sol-gel transition temperatures and the elastic modulus slightly decreased with increasing concentration of either NaCl or CaCl₂. The sol-gel transition temperatures and the elastic modulus measured for the polymer-salt gels are listed in Table 2.2. The possible explanation for these phenomena is: when the salts of NaCl and CaCl₂ form ions in water, the water molecules have more affinity for ions than the polymer molecules. In this case there is a decrease of the quantity of free water molecules. This system also has less water molecules to form bonds with the polymer molecules and the gelation process occurs at a lower temperature. The slightly decreased elastic modulus of

the solution containing NaCl and CaCl₂ is caused by a reduction in so weak quality for PEO, shrinking the micelle corona. The thermoreversible gelation behavior is generally accepted as a result of micellar close packing. When the salts are added into the solutions, the micelles become more packed with increase the salt concentration and could hardly occupy a high fraction volume of solution to come into contact and entangled with each other, consequently leading the weakened elastic modulus of the gels.

In Figure 2.11, we compare the effect of increasing the concentrations of clays and salts on the elastic modulus. The clay has a much larger effect on the modulus than the salts. G' increased by nearly a factor of two when the concentration of clay was increased to 1 % and decreased by ten percent when the concentration of either salt was increased to 2 %. In figure 2.12, we summarize the different effects of clays and salts on the sol-gel transition temperature, where we find that both salts and clays are effective in decreasing the transition temperature. In the case of salts, the decrease was described as being due to the 'salting' out effect where the salt and polymer compete for the water molecules.

2.4 Conclusion

Thermal gelation and structure of high concentration triblock copolymer poly(ethylene oxide)₉₉-poly(propylene oxide)₆₉-poly(ethylene oxide)₉₉(Pluronic

F127)-clay (Cloisite Na⁺ and Lucentite SWN) aqueous solutions were characterized by rheological measurements, differential scanning calorimetry (DSC) and small angle X-ray/neutron scattering. The sol-gel transition temperature, and the elastic modulus of the F127 solution were found to depend both on the concentration of polymer and of clay. Above the gel transition, the elastic modulus of the solutions increased with clay concentration. No change was observed for the yield strain of the polymer-clay gels. Two different kinds of inorganic salts, sodium chloride (NaCl) and calcium chloride (CaCl₂) were added into the polymer and polymer-clay solutions. The sol-gel transition temperature and elastic modulus of these systems decreased only a small amount with increasing concentration of inorganic salts. Addition of salts to polymer clay solutions resulted in precipitation of the clays which decreased the modulus. Neutron scattering was performed on 30 % F127 in DI water, with 1 % NaCl. In each case the scattering patterns corresponded to one crystal in the scattering volume with a distance of 19.2 nm between close packed micelles.

2.5 References

- [1] Cohn, D.; Sosnik, A.; Garty, S. *Biomacromolecules* **2005**, 6, 1168–1175.
- [2] Chun, K. W.; Lee, B. J.; Kim, S. H.; Park, T. G. *Biomaterials* **2005**, 26, 3319–3326.
- [3] Zhou, Z.; Chu, B. *J. Colloid Interface Sci.* **1988**, 126, 171–180.
- [4] Mortensen, K.; Pedersen, J. S. *Macromolecules* **1993**, 26, 805–812.
- [5] Wanka, G.; Hoffmann, H.; Ulbricht, W. *Macromolecules* **1994**, 27, 4145–4159.
- [6] Wanka, G.; Hoffmann, H.; Ulbricht, W. *Colloid & Polym Sci.* **1990**, 268, 101–117.
- [7] Wu, C.; Liu, T.; Chu, B.; Schneider, D. K.; Graziano, V. *Macromolecules* **1997**, 30, 4574–4583.
- [8] Prud'homme, R. K.; Wu, G.; Schneider, D. K. *Langmuir* **1996**, 12, 4651–4659.
- [9] Ricci, E. J.; Bentley, M.; Farah, M.; Bretas, R.; Marchetti, J. M. *European Journal of Pharmaceutical Sciences* **2002**, 17, 161–167.
- [10] Jorgensen, E. B.; Hvidt, S.; Brown, W.; Schillin, K. *Macromolecules* **1997**, 30, 2355–2364.
- [11] Pandit, N.; Trygstad, T.; Croy, S.; Bohorquez, M.; Koch, C. *Journal of Colloid and Interface Science* **2000**, 222, 213–220.
- [12] Mata, J.; Joshi, T.; Varade, D.; Ghosh, G.; Bahadur, P. *Colloids and Surfaces A* **2004**, 257, 1–7.

- [13] Jansson, J.; Schillen, K.; Nilsson, M.; Söderman, O.; Fritz, G.; Bergmann, A.; Glatter, O. *Journal of Physical Chemistry B* **2005**, 109, 7073–7083.
- [14] Sharma, P. K.; Matthew, J. E.; Bhatia, S. R. *Journal of Biomaterials Science-Polymer Edition* **2005**, 16, 1139–1151.
- [15] Matthew, J. E.; Nazario, Y. L.; Roberts, S. C.; Bhatia S. R. *Biomaterials* **2002**, 23, 4615–4619.
- [16] Edsman, K.; Carlfors, J.; Peterson, R. *Eur. J. Pharm. Sci.* **1998**, 6, 105–112.
- [17] Schmolka, I. *J. Biomed. Mater. Res.* **1972**, 6, 571–582.
- [18] Chu, B.; Harney, P. J.; Li, Y.; Linliu, K.; Yeh, F.; Hsiao, B. S. *Rev. Sci. Instrum.* **1994**, 65, 597–602.
- [19] Jiang, J.; Burger, C.; Li, C.; Lin, M. Y.; Rafailovich, M. H.; Sokolov, J. C., Manuscript in preparation.
- [20] Wu, C; Liu, T.; White, H.; Chu, B. *Langmuir* **2000**, 16, 656–661.
- [21] Giese, R. F.; Van Oss, C. J. *Colloid and surface properties of clays and related minerals* Marcel Dekker Inc. New York. 2002.

Table 2.1 The elastic modulus (37 °C) and sol-gel transition temperature for the Pluronic F127-Clay gels.

	Clay Concentration wt %	F127 concentration wt %	Elastic Modulus dyn/cm²	Sol-gel transition Temperature °C
SWN	0.00	30	8.17E-05	14.2
	0.13	30	8.65E-05	12.4
	0.25	30	1.09E-06	12.0
	0.50	30	1.33E-06	11.3
CNa	0.13	30	1.05E-06	13.2
	0.25	30	1.20E-06	12.7
	0.50	30	1.32E-06	12.4
	1.00	30	1.41E-06	11.8

Table 2.2 The elastic modulus (37 °C) and sol-gel transition temperature for the Pluronic F127-Salt gels.

	Salt concentration wt %	F127 concentration wt %	Elastic Modulus dyn/cm ²	Sol-gel transition Temperature °C
NaCl	0.00	30	8.17E-05	14.2
	0.50	30	7.94E-05	11.6
	1.00	30	7.63E-05	10.4
	1.50	30	7.06E-05	9.5
	2.00	30	6.66E-05	8.7
CaCl₂	0.00	30	8.17E-05	14.2
	1.00	30	8.17E-05	11.3
	1.50	30	7.78E-05	10.0
	2.00	30	7.23E-05	9.6

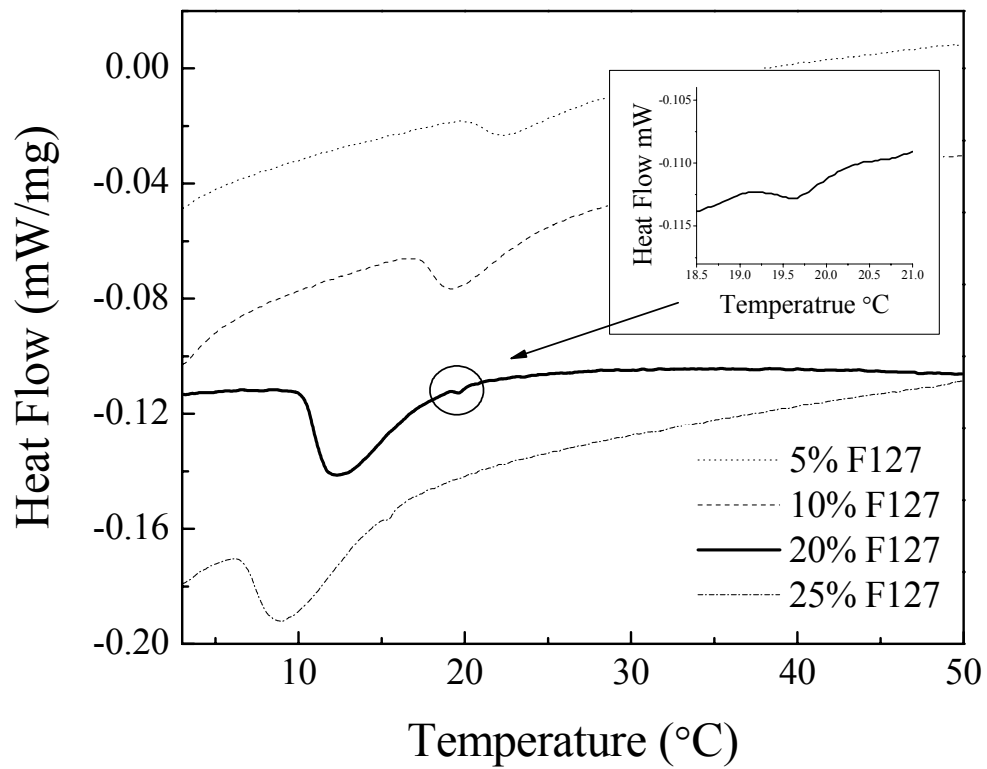


Figure 2.1 DSC-measurements on the different concentration solutions of Pluronic F127.

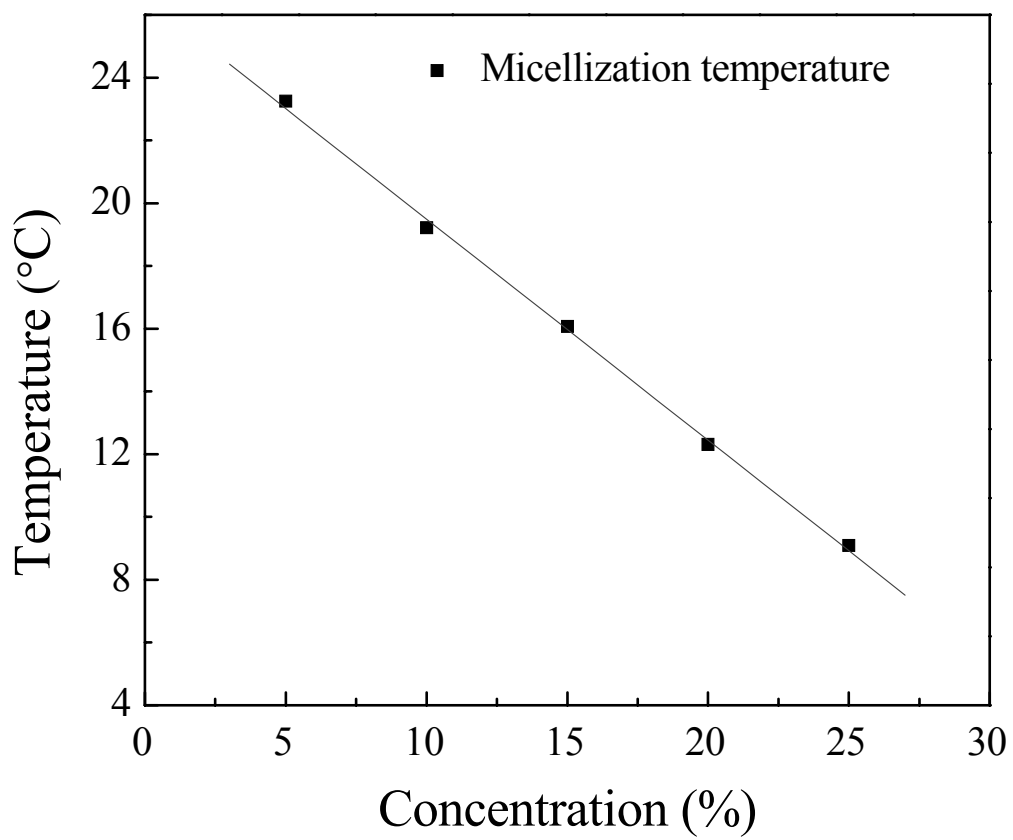


Figure 2.2 Micellization temperature as a function of the Pluronic F127 concentration.

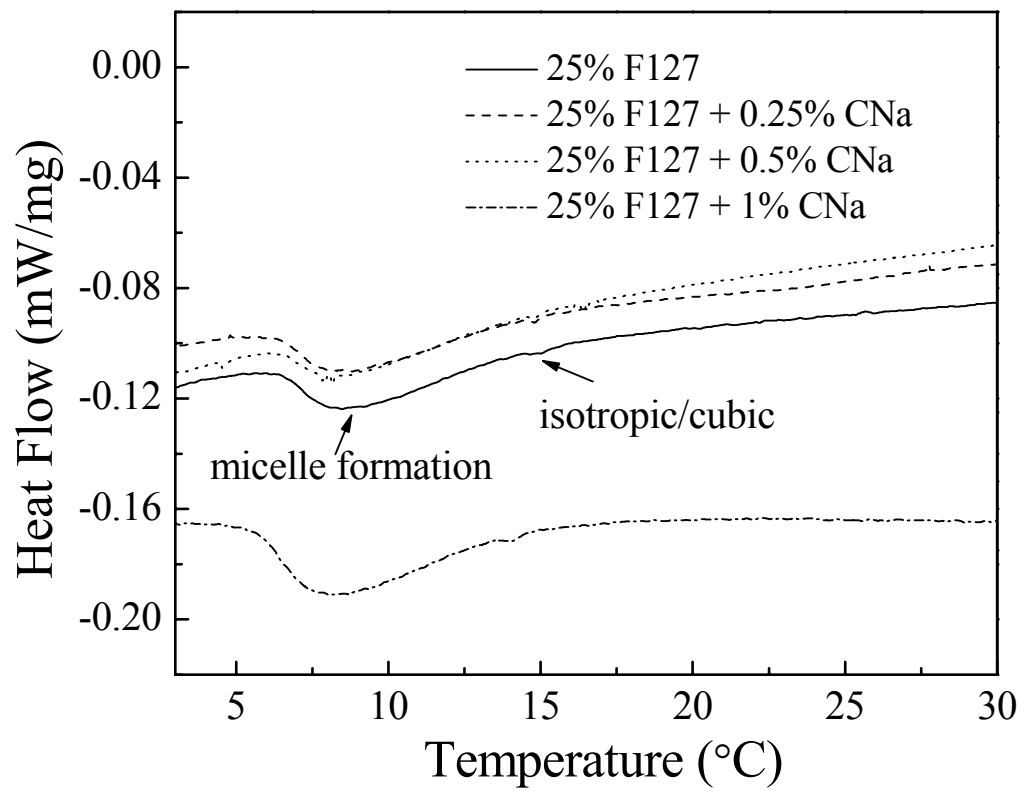


Figure 2.3(a) DSC-measurements on 25% F127 with CNa clay.

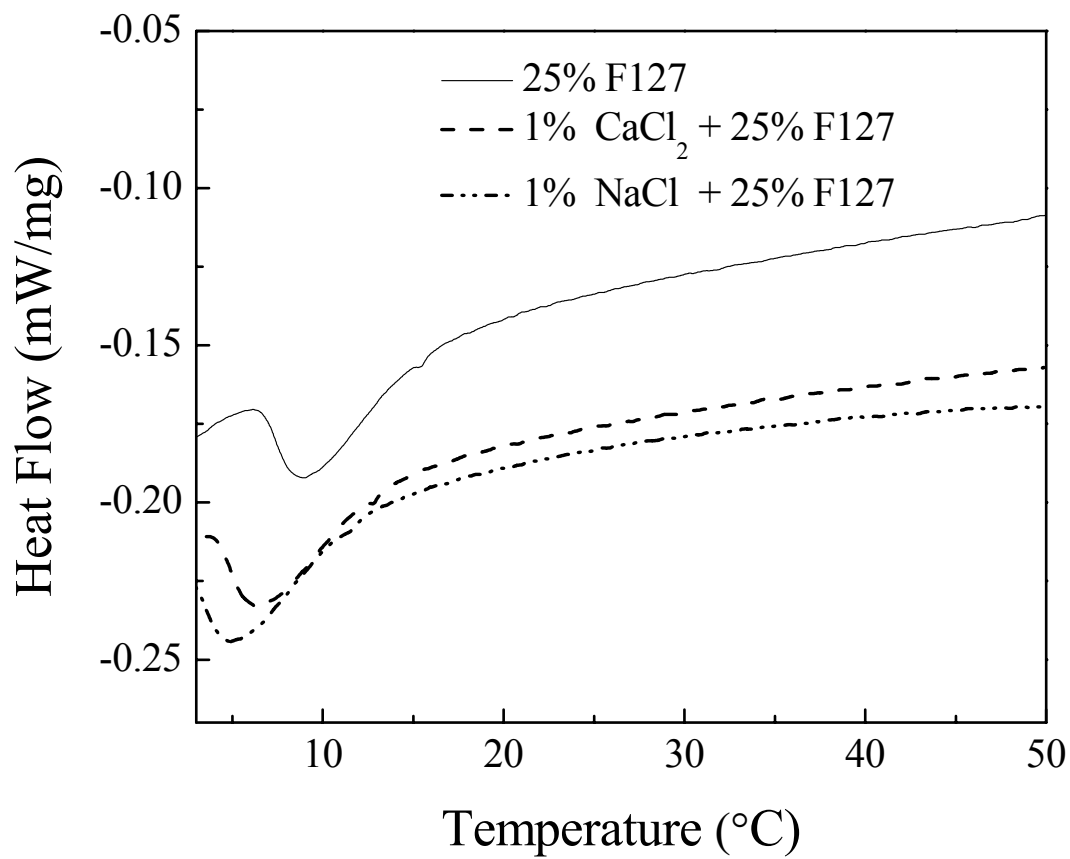


Figure 2.3(b) DSC-measurements on 25% F127 with CaCl₂ and NaCl salts.

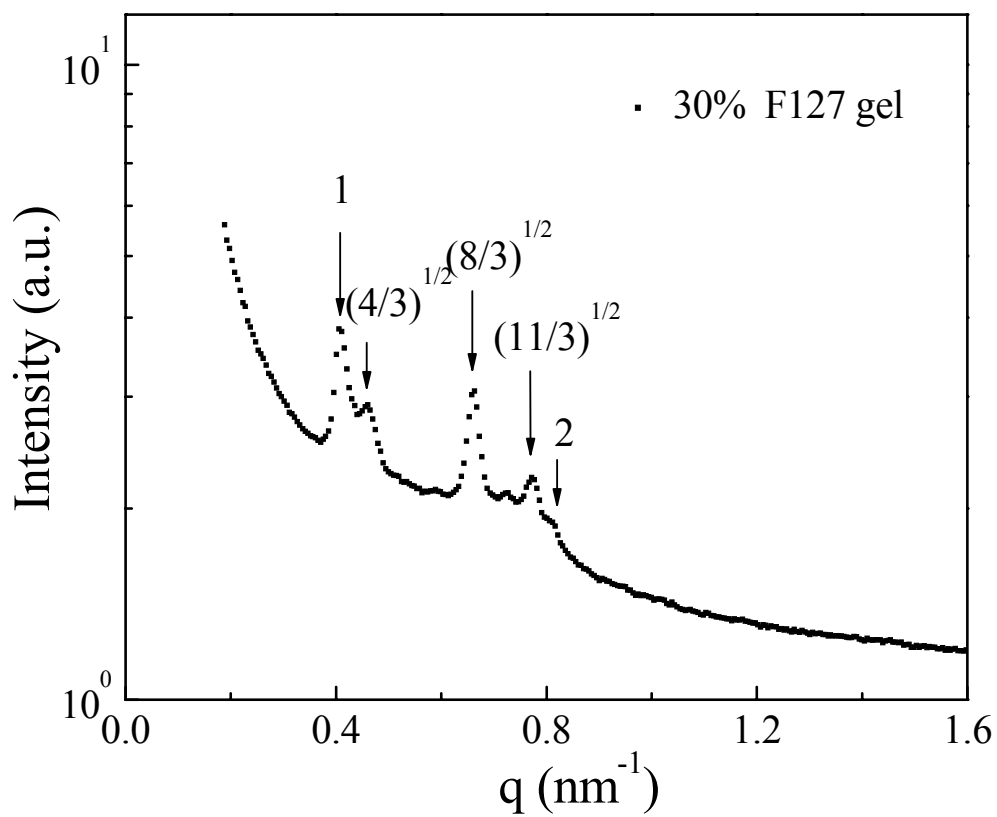


Figure 2.4 SAXS intensity profile of 30 wt % F127 in H₂O. The arrows indicate the peak positions. The numbers represent the ratio of the peak position relative to the first order peak.

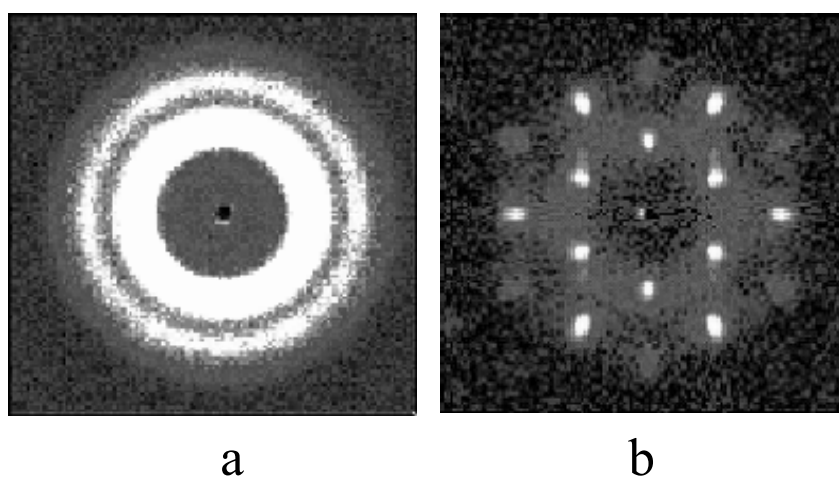


Figure 2.5 SANS intensity patterns of (a) 30 wt % F127 in D₂O; (b) 30 wt % F127 with 1 wt % NaCl in D₂O.

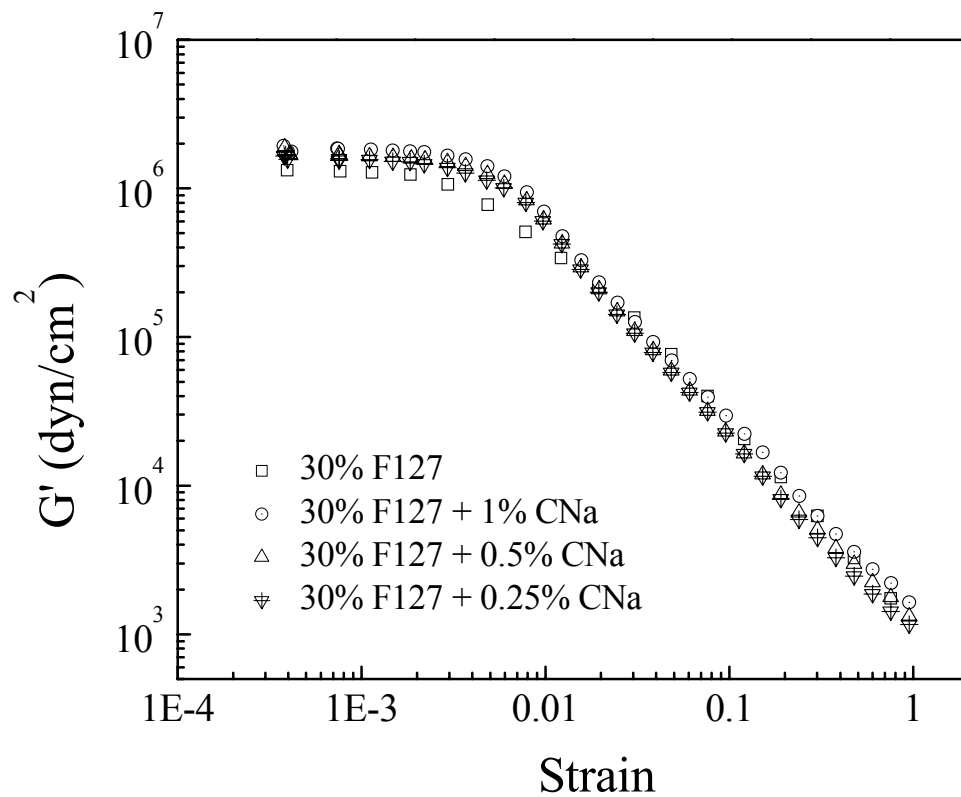


Figure 2.6 Elastic modulus as a function of strain for gels with 30 wt % Pluronic F127 with and without Cloisite Na⁺ (CNa) clay. The oscillating frequency is 1 rad/s and temperature is 37 °C. All have yield strain ~ 0.005.

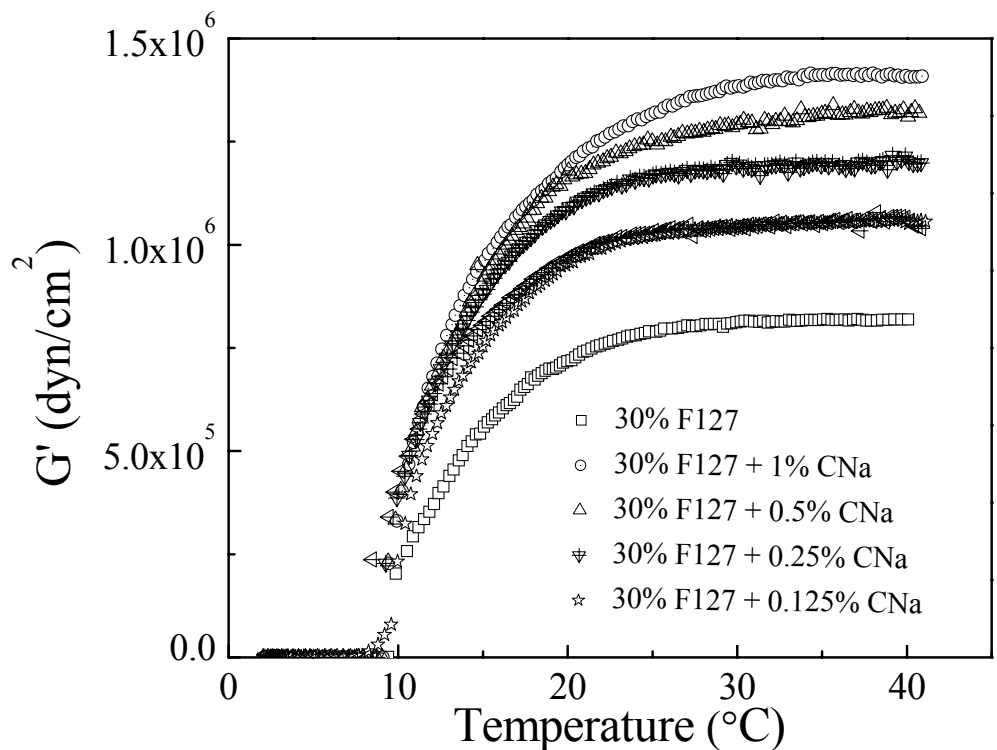


Figure 2.7 Storage modulus of 30% F127 during heating at 1°C/min, with and without Cloisite Na⁺ clay at a frequency of 1 rad/s and strain of 0.001.

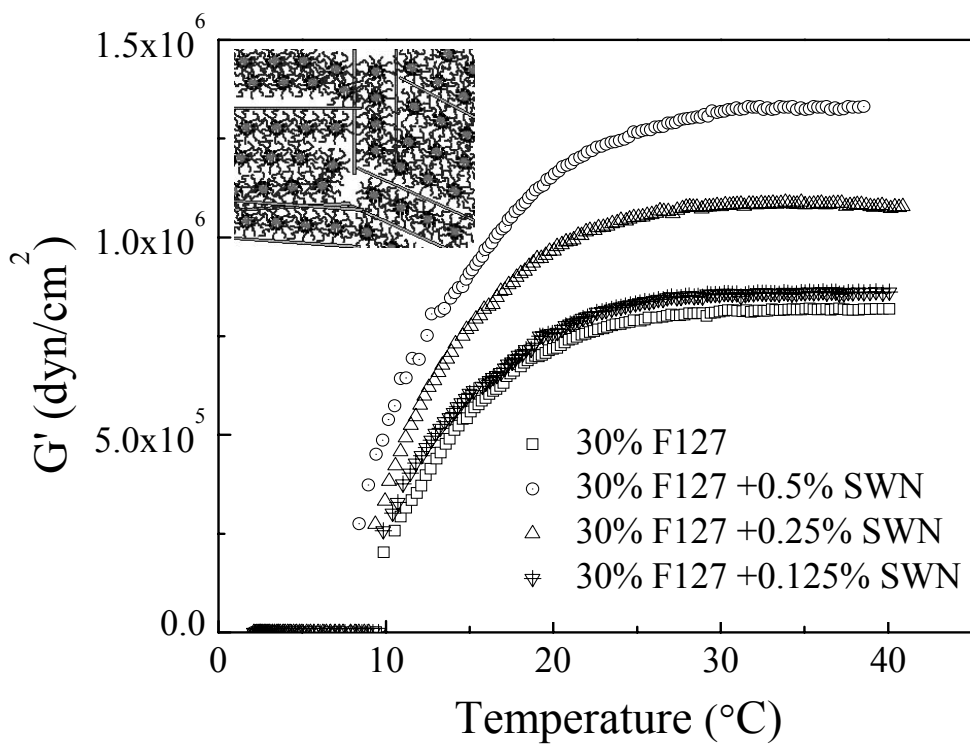


Figure 2.8 Storage modulus of 30% F127 during heating at $1^{\circ}\text{C}/\text{min}$, with and without SWN clay at a frequency of 1 rad/s and strain of 0.001 .

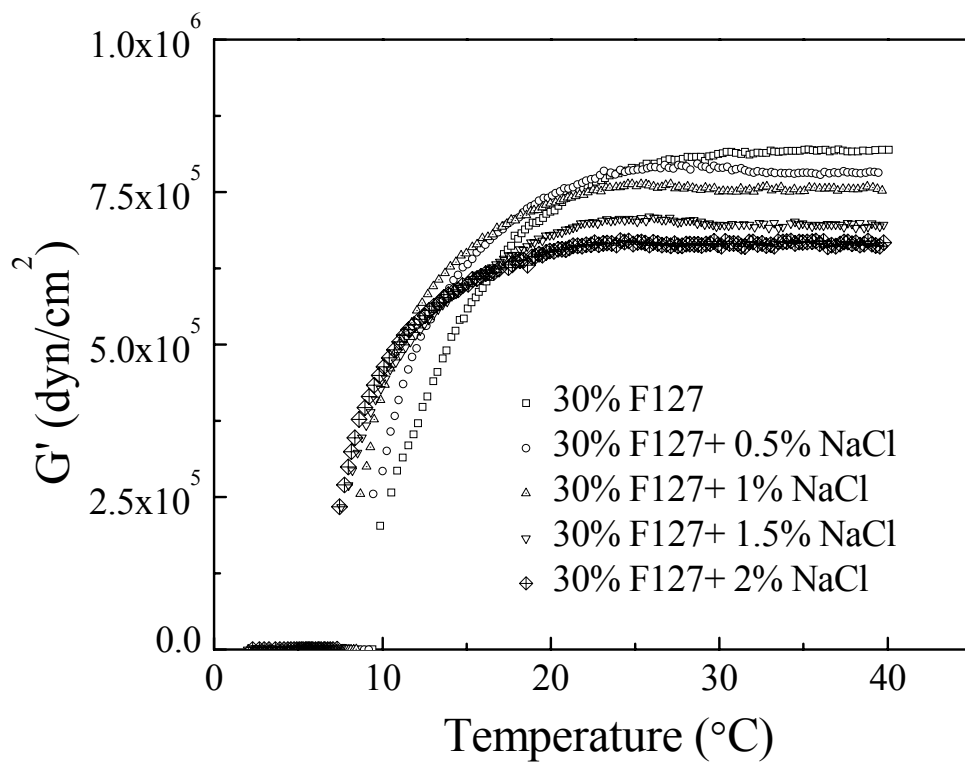


Figure 2.9 Storage modulus of 30% F127 during heating at 1°C/min, with and without NaCl at a frequency of 1 rad/s and strain of 0.001.

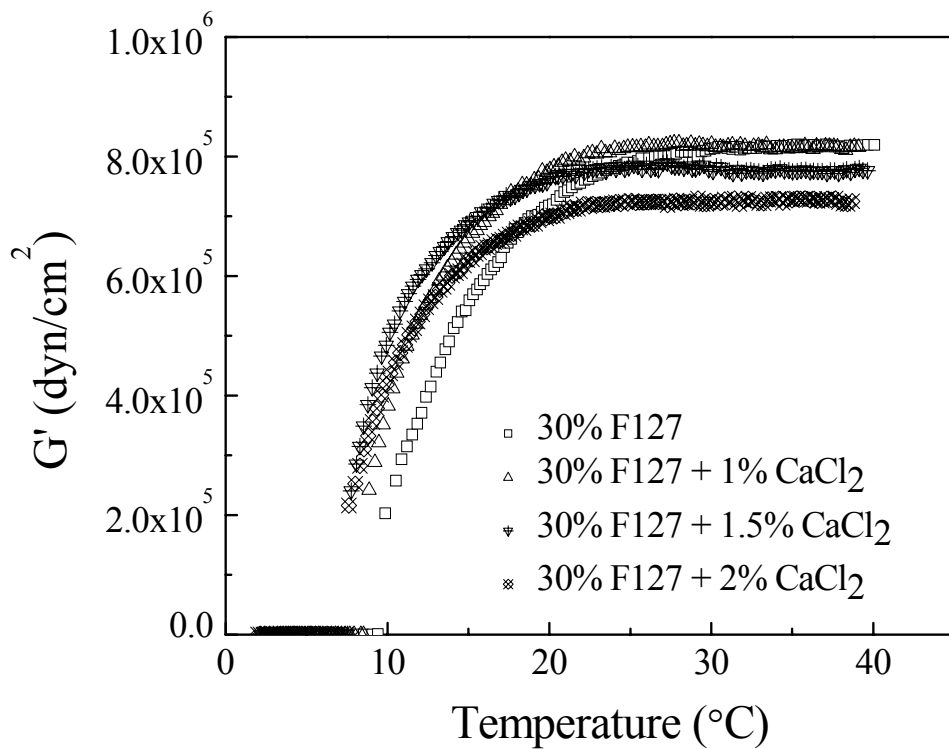


Figure 2.10 Storage modulus of 30% F127 during heating at 1°C/min, with and without CaCl₂ at a frequency of 1 rad/s and strain of 0.001.

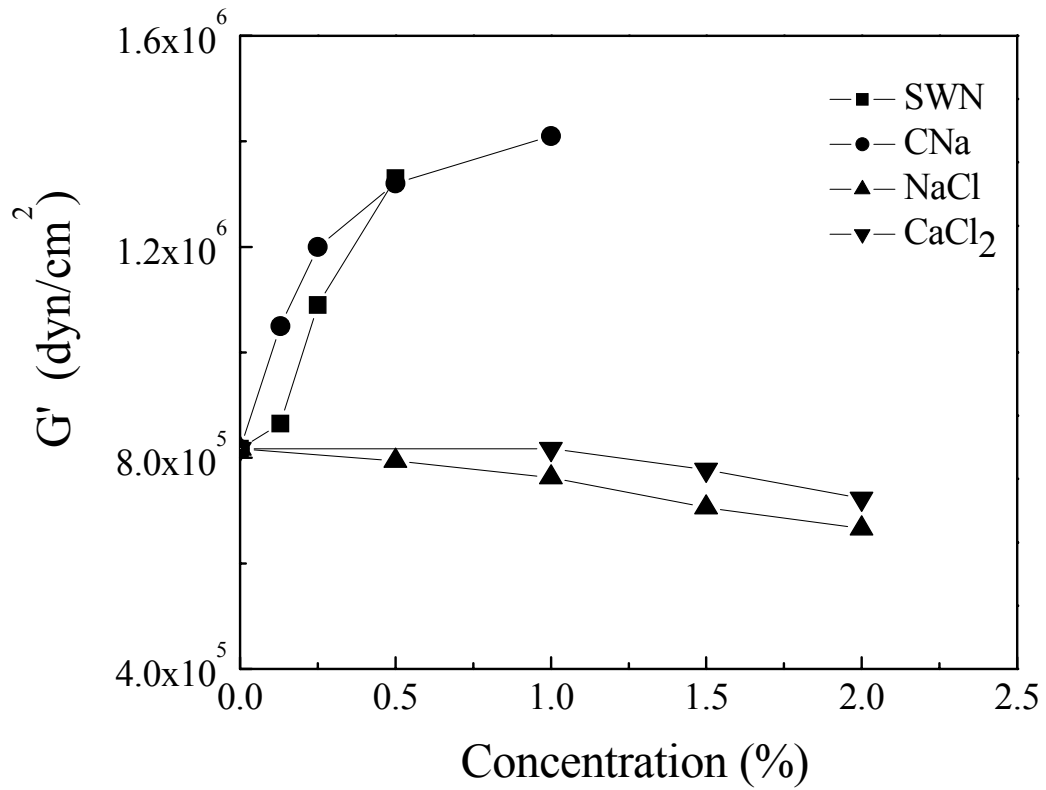


Figure 2.11 Elastic modulus of the gel as a function of the additive concentration. Clays raise the modulus, while salts subtly lower the modulus.

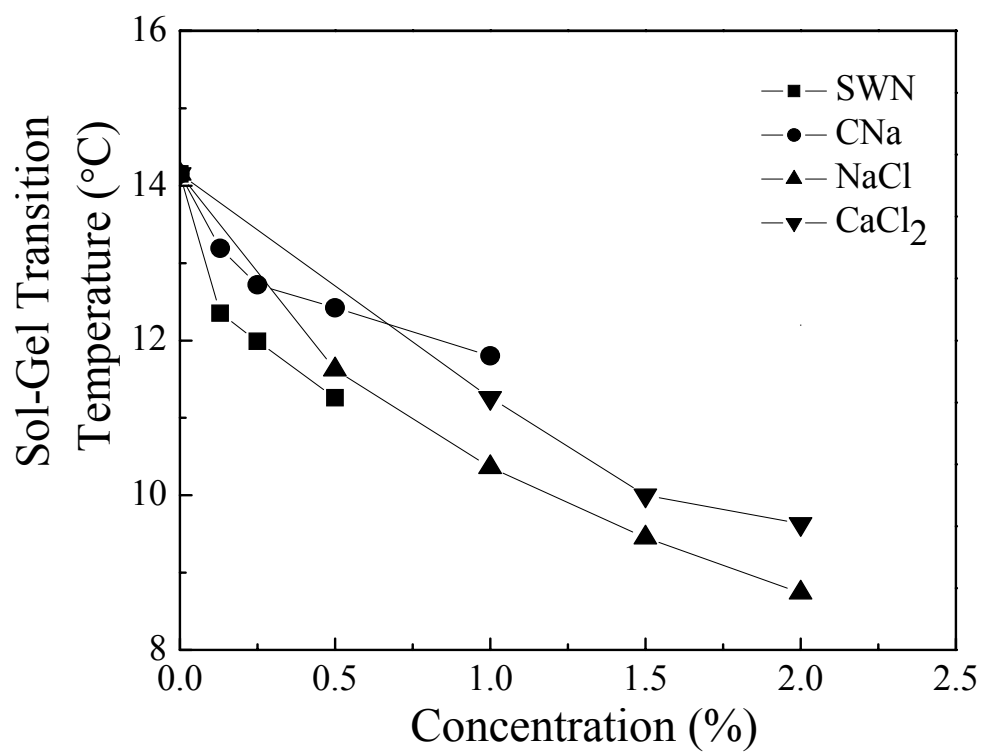


Figure 2.12 The sol-gel transition temperature as a function of the additive concentration.

CHAPTER 3

Shear Induced Layered Structure of Polymeric Micelles by SANS

(Published on *Macromolecules* 2007)

3.1 Introduction

Due to their thermoreversible gelation property, concentrated solutions of non-ionic amphiphilic triblock copolymers like poly(ethylene oxide)₉₉ - poly(propylene oxide)₆₉ -poly(ethylene oxide)₉₉ (PEO₉₉-PPO₆₉-PEO₉₉, Pluronic F127) are being widely used in numerous biomedical applications, such as drug delivery, gels for replacing biological fluids [1,2]. While most traditional polymer gels are formed by a swollen network of covalently cross-linked polymer chains, the present triblock copolymer gel is held together by reversible entanglements between the coronae of neighboring micelles [3-6]. The reversible nature of the entanglements is due to the absence of covalent cross-linking between the micelles. The organization of micelles into layers adapted to laminar shear flow is responsible for the exceptional visco-elastic properties of these systems, especially when being subjected to shear forces. Consequently the structure property relationships are dynamic and vary with the shear rate. Hence, it is

important to understand their correlation with rheology as a function of the shear rate.

Since the pioneering work of Hoffman, Ackerson and Loose [7-9] on shear-induced transitions in suspensions of charged particles, much effort has been made to identify the structural properties of colloidal crystals under shear. More recently [10,11], it has been shown that the selective solvent properties of diblock or triblock copolyethers like polyethylene oxide (PEO), polypropylene oxide (PPO) or polybutylene oxide (PBO) in aqueous solution can lead to the formation of micelles with a spherical core-shell geometry (Figure 3.1a). While dilute solutions contain discrete micelles, concentrated solutions can form highly ordered arrangements of micelles, characterized by a certain overlap of the coronae of neighboring micelles (Figure 3.1b–d). Especially in a shear environment, the packing order is dominated by 2D hexagonally packed layers of micelles (Figure 3.1b), the vertical stacking of which approaches 3D close packings of spheres with the limiting cases of perfect ABC stacking sequence (Figures 3.1d and 2a), corresponding to a face-centered cubic (FCC) structure, and perfect ABA stacking leading to the 3D hexagonally close packed structure (Figure 3.2b), respectively, and their intermediates ranging from near ideal structures with moderate stacking faults to random stacking sequences (Figure 3.2c) As far as the structure under shear flow is concerned, a link has been established between the former conventional (charge-stabilized) colloidal crystals

and the latter non-ionic micellar close packed phases. The ordering would drastically influence the flow properties of the dispersion because the layered structure would comply easily with the flow, thereby reducing the shear viscosity. This effect is known as “shear thinning.”

To build a 3D close packing of spheres, starting from a single 2D hexagonally packed layer of micelles (A), Figure 3.1b, and adding a second layer (B), Figure 3.1c, there are two possibilities for the addition of the next layer, either filling the “holes” visible in the projection (C), Figures 3.1d and 3.2a, leading to an ABC stacking sequence, corresponding to a face-centered cubic (FCC) structure, or reverting back to the shift of the first layer (A), not depicted in Figure 3.1, leading to an ABA stacking sequence or 3D close-packed hexagonal structure, Figure 3.2b. The addition of further layers could proceed in an ordered fashion replicating an ABCABC or ABABAB stacking sequence, or it could involve stacking faults, Figure 3.2c. From a comparison of Figure 3.1d and Figures 3.2a–c it is clear, that the nature of the stacking order becomes much more obvious in the Figures 3.2, viewed parallel to layer planes, rather than for Figure 3.1d viewed perpendicular to the layer planes, where most information about the stacking sequence is lost in the projection.

It is crucial to understand that this situation directly translates to a scattering experiment in Couette shearing geometry, Figure 3.3. As expected, the layers of micelles are found to be arranged parallel to the cylinder surfaces of the outer and

inner concentric Couette cylinders. Thus, the traditional Couette scattering geometry with the neutron beam centered at the Couette cell (“radial” geometry, Figure 3.3) corresponds to the perpendicular situation of Figure 3.1d, so that most information about the stacking sequence is lost in the projection onto the plane normal to the beam. In order to extract the stacking sequence information, an experiment in “tangential” geometry (Figure 3.3), corresponding to Figure 3.2, needs to be performed.

The system that we have investigated under shear is a ‘soft solid’, resulting from the aggregation of self-assembling triblock copolymers-PEO₉₉-PPO₆₉-PEO₉₉ into spherical core-shell micelles, Figure 1a, and crystallizing into a 3D close packed macro-lattice [3,4]. The spherical micelle consists of a core of mainly the comparatively more hydrophobic PPO blocks (shown as dark in Figures 3.1 and 3.2) with a low water content, surrounded by a water-swollen corona of PEO-blocks (shown as light in Figures 3.1 and 3.2). At low polymer concentrations, light scattering measurements corroborate the aggregation of copolymers into spherical micelles and allow the determination of the micelle size. In the gel-like region the aggregation number (60–65) and also the micellar core radius size (4–5 nm) are not sensitive to concentration or temperature changes [3].

The oriented structures of several similar copolymers under steady shear have been studied by SANS and SAXS [12-17]. For instance, using scattering techniques on both tangential and radial geometry, Molino, Diat and Slawacki et

al [12-15], showed the shear orientation effects on the micelle system of Pluronic F85 and F108. In this work, we present several extensions to the theoretical scattering analysis by Loose and Ackerson [8,9] on which all previous data evaluation was based, and apply it to experimental SANS data under shear for the F127 copolymer system.

3.2 Experimental Section

Pluronic F127 (12 600 Daltons, 70% w/w PEO) was obtained from BASF (Mount Olive, NJ, USA). Concentrations of Pluronic F127 solutions are expressed by weight percentage (% w/w). Pluronic was dissolved in deuterium oxide, obtained from Cambridge Isotope Laboratories, Inc., and kept stirring in an ice water mixture at 2 °C for 2 hours. The solution was then refrigerated for 1–2 days until it cleared. Deuterium oxide was used to obtain good contrast and low background in the neutron scattering experiments.

The small angle neutron scattering (SANS) experiments were performed at the national institute of standards and technology (NIST) reactor division. Data were collected on an area sensitive detector at the NG3 (NIST/Exxon/U.Minn) SANS beamline, with sample-to-detector distances of 3.45 m. The nominal wavelength of the neutrons was 0.60 nm with a dispersity $\Delta\lambda/\lambda$ of 0.10 and an average incident intensity of approximately 464 000 neutrons/s, the accessible q -

range was from 0.055 to 0.969 nm⁻¹, and the magnitude of the scattering vector is defined by $q = (4\pi/\lambda)\sin(\theta/2)$, where θ is the angle between incident and scattered beam. The micellar solutions were placed inside a Couette apparatus designed for SANS experiments. This quartz Couette shearing setup consists of a fixed diameter rotor with several choices for the internal stator. The resulting scattering configuration for the steady shear experiments is outlined in Figure 3. The Couette cylinder could be shifted such that the incident beam could pass through the radial or the tangential sample position, providing two different views of the structure corresponding to Figures 3.1 and 3.2, respectively. We chose a stator offering a 1 mm gap width. Samples were loaded carefully at 2 °C to minimize shear effects. Then the temperature was increased to 37 °C, where the sample was stabilized for 20 min before the onset of shear. The diffraction images represent the steady shear microstructure at the prescribed shear rate averaged over a 5–10 min integration time.

The steady shear stress versus shear rate data were collected from a strain-controlled rheometer, Rheometrics Fluids Spectrometer II, using concentric cylinders with an inner diameter of 16.5 mm, an outer diameter of 17.1 mm and 13.7 mm height. Temperature control was achieved using a water bath with concentric cylinders, and the temperature was determined from a thermocouple connected to the inner cylinder. Low viscosity silicone oil was added on top of the surface of the sample to minimize evaporation of the solvent.

Scattering Theory

The scattered intensity I of a system of stacked layers can be factorized into three components,

$$I(\mathbf{q}) = F(\mathbf{q}) L(\mathbf{q}) Z(\mathbf{q}) \quad (1)$$

where F is the form factor of a single micelle, L is an intra-layer lattice factor describing the arrangement of the micelles inside a single layer, and Z is an inter-layer lattice factor describing the arrangement between the layers.

The scattering vector \mathbf{q} has the absolute value $q = |\mathbf{q}| = 4\pi \lambda^{-1} \sin(\theta/2)$ where θ is the angle between incident and scattered beam and λ is the wavelength, and it has the components $\mathbf{q} = (q_1, q_2, q_3)$ where q_1 points tangentially in the Couette shear flow direction, q_2 points into the direction of the Couette rotation axis, and q_3 points radially perpendicular to the Couette shear flow direction, see Figure 3.3. Thus, in a Couette SANS experiment in *radial geometry*, we will measure a planar 2D section (neglecting Ewald sphere curvature effects) in the (q_1, q_2) plane with $q_3 = 0$ through the total intensity distribution (1) in reciprocal space, and in *tangential geometry*, we will measure a section in the (q_3, q_2) plane with $q_1 = 0$.

Without significant loss of generality, we approximate the micelle form factor by its Guinier approximation

$$F(\mathbf{q}) = F(q) = \exp(-R_G^2 q^2 / 3) \quad (2)$$

where R_G is the radius of gyration, assuming that form factor minima and oscillations are averaged out due to polydispersity effects and due to the core-

shell nature of the micelle, and because the experimental q -range is small enough. Eq. (2) sufficiently describes our data, and for specific density profiles of the core and corona regions, the corresponding R_G could be calculated and compared with the one obtained from (2). Explicit expressions for the form factors of various core-shell morphologies are given in ref 18, but their use is not really warranted for the present data.

Inside a single layer of micelles, we assume a 2D hexagonal close packed arrangement described by the real space unit cell vectors

$$\mathbf{a} = (1, \sqrt{3}, 0) a / 2 \quad \text{and} \quad \mathbf{b} = (1, -\sqrt{3}, 0) a / 2 \quad (3)$$

where a is the center-to-center distance between neighboring micelles, corresponding to a set of reciprocal space unit cell vectors

$$\mathbf{a}^* = (1, 1/\sqrt{3}, 0) 2\pi / a \quad \text{and} \quad \mathbf{b}^* = (1, -1/\sqrt{3}, 0) 2\pi / a \quad (4)$$

Note that there are two possible orientations for an aligned 2D hexagonal lattice, the unit hexagon standing on its edge or standing on its tip, respectively, and the on-edge orientation as depicted in Figure 1a and as defined by (3) and (4) for real and reciprocal space corresponds to the experimentally observed one, as follows from the agreement of the orientation of experimental and calculated radial patterns, see Figures 3.5 and 3.6.

For the 2D hexagonal arrangement defined by these unit cell vectors, the intra-layer lattice factor L is given by

$$L(\mathbf{q}) = \sum_{h=-\infty}^{\infty} \sum_{k=-\infty}^{\infty} w_{hk}^{-2} \exp(-\pi w_{hk}^{-2} |\mathbf{q} - h\mathbf{a}^* - k\mathbf{b}^*|^2) \quad (5)$$

where we have assumed the individual peak shapes to be given by Gaussians of integral widths w_{hk} which may depend on the Miller indices h and k . It would be straightforward to use different peak shapes, but Gaussians appear to work well for our experimental data.

In order to speed up the calculation, we replace the exact expression (5) by the approximation

$$\tilde{L}(\mathbf{q}) = w_{hk}^{-2} \exp\left(-\frac{\pi^2}{a^2 w_{hk}^2} \times \left\{ \sin^2\left[\frac{aq_1}{2}\right] + \sin^2\left[\frac{a}{4}(q_1 + \sqrt{3}q_2)\right] + \sin^2\left[\frac{a}{4}(q_1 - \sqrt{3}q_2)\right] \right\}\right) \quad (6)$$

which is good for sufficiently narrow and well-separated peaks and calculates much faster than the original (5).

Assuming the average distance from one layer to the next is that of an ideal close packing of spheres, so that neighboring micelles between layers also have a center-to-center distance a , there are two possible translation vectors

$$\mathbf{t}_1 = (0, 1/\sqrt{3}, \sqrt{2/3})a \quad \text{and} \quad \mathbf{t}_2 = (0, -1/\sqrt{3}, \sqrt{2/3})a \quad (7)$$

which describe the relative positioning from one layer to the next. If the inter-layer distance deviates from the ideal value, (7) can be adjusted accordingly. Translational disorder can be introduced by displacing the translation vectors $\mathbf{t}_{1,2}$

by vectors $(\Delta_1, \Delta_2, \Delta_3)$ where the displacement components $\Delta_{1,2,3}$ can be different for different directions of space and are taken to be normally distributed with standard deviations $\sigma_{1,2,3}$. This adjustable translational disorder can be used to analytically describe the effects of layer sliding or, after a straightforward modification of (9), for a “zig-zag path” movement of the layers. Note that this constitutes a significant step beyond the treatment of Loose and Ackerson [9] who consider discrete translational displacements only. Curiously, Molino et al [14] using the Ackerson-Loose treatment describe the generalization to a continuum of displacements as a “formidable task” while the present work shows that it is, in fact, a minor modification, e.g., by extending the well-known chain of independent events model by Hermans [19] to the following dependent statistics.

In order to take stacking sequence correlations in first order into account, we assume that the layer stacking sequence can be described by a first order Markov process. Its lattice factor can be summed in close form using matrix techniques [20]. Let the probability that a translation \mathbf{t}_j be followed by a translation \mathbf{t}_k be given by p_{jk} where j and k can assume the values 1 or 2. Since $p_{j1} + p_{j2} = 1$ there are only two independent probabilities, say p_{11} and p_{22} . The probability p_j of finding a translation vector \mathbf{t}_j can be obtained from $p_j = p_1 p_{1j} + p_2 p_{2j}$ and $p_1 + p_2 = 1$. Under these conditions, the inter-layer lattice factor $Z = Z(\mathbf{q})$ is given by

$$Z = 1 + 2 \operatorname{Re} \left\{ \begin{pmatrix} p_1 & H_1 \\ p_2 & H_2 \end{pmatrix}^T \left[\begin{pmatrix} 1 & 0 \\ 0 & 1 \end{pmatrix} - \begin{pmatrix} p_{11}H_1 & p_{12}H_2 \\ p_{21}H_1 & p_{22}H_2 \end{pmatrix} \right]^{-1} \begin{pmatrix} 1 \\ 1 \end{pmatrix} \right\} \quad (8)$$

where

$$H_j(\mathbf{q}) = \exp\left[i\mathbf{q}\mathbf{t}_j - (\sigma_1^2 q_1^2 + \sigma_2^2 q_2^2 + \sigma_3^2 q_3^2)/2\right] \quad (9)$$

is the Fourier transform of the distribution of translations of the j type including their disordering displacements.

Note that (8) differs from eq. A2 in Loose and Ackerson [9] where those authors incorrectly assume $p_1 = p_2 = 1/2$ to be valid in the general case. Setting $p_1 = p_2$ implies $p_{11} = p_{22}$, a specialization Loose and Ackerson eventually introduced in their eq. A7 so that their final result is correct again within this limitation, but the exact general solution (8) or (10), even including the generalization to continuous sliding, is not much more complicated than Loose and Ackerson's expressions. The specialization $p_{11} = p_{22}$ assumes that all regions with predominantly ABC stacking sequences are accompanied by equal amounts of ACB regions (twinning) and appears unmotivated in the present anisotropic shear environment; it is, in fact, not compatible with some of our data obtained in tangential Couette geometry (see e.g. the first pattern in Figure 3.7) which is much more sensitive to these effects than the traditional radial geometry.

Eq. (8) can be rewritten in the following form which is directly suitable for the calculation:

$$Z = \text{Re}\{2 - p_{11} - p_{22} + [2 - (p_{11} + p_{22})(2 - p_{11})]H_1 + [2 - (p_{11} + p_{22})(2 - p_{22})]H_2 + (1 - p_{11} - p_{22})(2 - p_{11} - p_{22})\}$$

$$\times \{(2 - p_{11} - p_{22})[1 - p_{11}H_1 - p_{22}H_2 - (1 - p_{11} - p_{22})H_1H_2]\}^{-1} \quad (10)$$

3.3 Results and Discussion

Figure 3.4 shows the steady shear viscosity as a function of the shear rate for the micellar gel of 20% F127 in water. From the figure we can see that the viscosity decreased with increasing shear rate, i.e., the gel is a shear thinning system. The insert of oscillatory frequency sweep shows that this material is in fact a solid. This result had been previously reported by Prud'homme *et al* who described the shear rate dependence of the viscosity of such non-Newtonian fluids by using a Carreau-like model, $\eta = \eta_0 / (1 + (a\dot{\gamma})^b)$ where a and b are two coefficients related to volume fraction and properties of the micelles [21]. This decrease of the viscosity indicates that the 2D hexagonally close-packed layers of micelles form shear planes which are arranged to minimize the resistance against laminar flow.

Figures 3.5 a–i show the experimental scattering patterns of 20% F127 in D₂O, obtained in the radial scattering geometry, with increasing shear rate from 0 to 600 1/s. The corresponding tangential scattering patterns are shown in Figure 3.7 a–i.

The model discussed in the theoretical section allows the calculation of 2D SANS scattering patterns that can be compared to the experimental data. Figures 3.6 and 3.8 show calculated patterns for radial and tangential scattering geometry, respectively, with parameters semi-quantitatively adjusted by trial and error to produce the best visual agreement with the experimental patterns. Many of the structural parameters of interest are quite sensitive to small changes and can be obtained with good accuracy from these comparisons (e.g., micelle center-to-center distance a error $< 1\%$, micelle core radius R error $< 5\%$). The stacking sequence probabilities p_{11} and p_{22} are less sensitive, especially in radial scattering geometry (for the tangential patterns we would estimate an error around $< 20\%$).

Furthermore, it was found to be necessary to include an isotropic component in form of one or two scattering rings in the calculated patterns. As a function of the shear rate, the volume fraction of the isotropic component decreased from about 0.999 for zero shear to about 0.7 for a shear rate of 600 1/s, indicating a continuing transformation of unoriented domains into the shear-aligned orientation.

The stacking sequence probabilities were found to change from $p_{11}=0.9$ and $p_{22}=0.7$ (Figure 3.8a) for a zero shear rate down to $p_{11}=0.5$, $p_{22}=0.5$ (Figure 3.8i) for the shear rate of 600 1/s. This change of the stacking sequence probabilities suggests a structure change from asymmetrically twinned ABC (FCC) at low shear rates to a random AB stacking sequence at high shear rates. The clear

texture (Figure 3.7a) observed in samples exposed to zero shear could be due to surface-induced micelle crystallization at the cylinder surface during the gelation process when increasing the temperature from 2 to 37 °C [22]. Note again that most of this information cannot be obtained in radial scattering geometry.

The intra-layer neighboring micelle center-to-center distance a depends on the concentration of the polymer. By analyzing the experimental scattering patterns, we found that the distances between intra-layer neighboring micelle are 20.5 nm and 19.2 nm for 20% and 30% polymer solutions, respectively. From these numbers, we can see that the micelle distance gets smaller due to the closer packing of micelles by increasing the polymer concentration. This distance did not change as a function of the shear rate.

The inter-layer neighboring micelle center-to-center distance $|t_1|=|t_2|$ only influences the tangential patterns and has no effect on the radial patterns. From the experimental tangential patterns, we found no need to adjust this parameter from its ideal value a for a 3D close packing of spheres.

The stacking sequence translational shift parameters σ_1 , σ_2 and σ_3 were all taken to be 1 nm for most calculated patterns, indicating a moderate amount of translational disorder both parallel and perpendicular to the shearing planes.

The micellar core radius of gyration R_g (assuming an idealized core-shell scattering length density profile; for a more realistic non-constant corona density

profile, this is to be understood as some sort of apparent or equivalent radius) was found as $R_g = 6.5$ nm, independent of the shear rate.

It is conceivable that under shear the micellar cores could deform from an ideal spherical to an ellipsoidal shape. This effect could be taken into account by subjecting the micellar form factor to the reciprocal deformation. Within the accuracy of our experiments and analysis, an undeformed micelle form factor was found to sufficiently describe the experimental data. Thus, we did not observe this type of deformation. The layered structure was stable even up to shear rates of 1000 1/s.

3.4 Conclusion

Small angle neutron scattering (SANS) experiments in radial and especially tangential scattering configurations were performed to examine the shear rate dependence of the micellar macro-lattice formed by concentrated aqueous solutions of triblock copolymer-poly(ethylene oxide)₉₉-poly(propylene oxide)₆₉-poly(ethylene oxide)₉₉ (Pluronic F127), subjected to in situ steady shear. The micellar gel showed a shear thinning behavior to reduce the resistance to shear by forming a layered stacking of two-dimensional HCP micelles. An experiment in “tangential” scattering provided us the most stacking sequence information. A theoretical model was developed to calculate the scattering intensity distribution

in 3D reciprocal space for oriented stacks of micellar layers with stacking sequences following a first order Markov process, allowing for disorder effects and having ideal cubic and hexagonal close packings as its limiting cases. 2D sections through these calculated 3D intensity distribution were compared to experimental SANS scattering patterns. The model developed could be applied to other systems, such as layered packings of ionic copolymer micelles or other particles, and also to non-particulate layered systems like graphite or clay. The ability to understand the essential relationships between hydrogel structure and its rheological response could have numerous applications for hydrogel implants under physiological conditions.

3.5 References

- [1] Chun, K. W.; Lee, J. B.; Kim, S. H.; Park, T. G. *Biomaterials* **2005**, 26, 3319–3326.
- [2] Cohn, D.; Sosnik, A.; Garty, S. *Biomacromolecules* **2005**, 6, 1168–1175.
- [3] Wu, C.; Liu, T; Chu, B.; Schneider, D. K.; Graziano, V. *Macromolecules* **1997**, 30, 4574–4583.
- [4] Mortensen, K.; Talmon, Y. *Macromolecules* **1995**, 28, 8829–8834.
- [5] Wanka, G.; Hoffmann, H.; Ulbricht, W. *Macromolecules* **1994**, 27, 4145–4159.
- [6] Mortensen, K. *J. Phys.: Condens. Matter* **1996**, 8, A103–A124.
- [7] Hoffman, R. L. *Trans. Soc. Rheol.* **1972**, 16, 155–173.
- [8] Ackerson, B. J.; Clark, N. A. *Phys. Rev. Lett.* **1981**, 46, 123–126.
- [9] Loose, W.; Ackerson, B. J. *J. Chem. Phys.* **1994**, 101, 7211–7220.
- [10] Castelletto, V.; Hamley, I. W.; Holmqvist, P.; Rekasas, C.; Booth, C.; Grossmann, J. G. *Colloid. Polym. Sci.* **2001**, 279, 621–628.
- [11] Daniel, C.; Hamley, I. W.; Mingvanish, W.; Booth, C. *Macromolecules* **2000**, 33, 2163–2170.
- [12] Diat, O.; Porte, G; Berret, J. -F. *Physical Review B* **1996**, 5, 14869–14872.
- [13] Berret, J.-F.; Molino, F. R.; Porte, G.; Diat, O.; Lindner, P. *J. Phys.: Condens. Matter* **1996**, 8, 9513–9517.

- [14] Molino, F. R.; Berret, J.-F.; Porte, G.; Diat, O.; Lindner, P. *Eur. Phys. J. B* **1998**, 3, 59–72.
- [15] Slawecki, T. M.; Glinka, C. J.; Hammouda, B. *Physical Review E* **1998**, 58, R4084–R4087.
- [16] McConnell, G. A.; Lin, M. Y.; Gast, A. P. *Macromolecules* **1995**, 28, 6754–6764.
- [17] Hamley, I. W. *J. Phys.: Condens. Matter* **2001**, 13, 643–671.
- [18] Förster, S.; Burger, C. *Macromolecules* **1998**, 31, 879–891.
- [19] Hermans, J. J. *Rec. Trav. Chim. Pay-Bas* **1944**, 63, 211–218.
- [20] Hendricks, S.; Teller, E. *J. Chem. Phys.* **1942**, 10, 147–167.
- [21] Prud'homme, R. K.; Wu, G.; Schneider D. K. *Langmuir* **1996**, 12, 4651–4659.
- [22] Wu, C.; Liu, T.; White, H.; Chu, B. *Langmuir* **2000**, 16, 656–661.

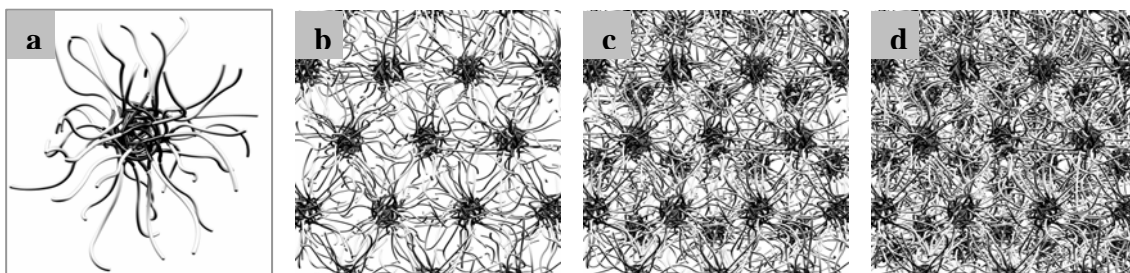


Figure 3.1 Schematic representations of Pluronic F127 micelles: (a) single micelle with spherical core-shell geometry; (b) single 2D hexagonally packed layer of micelles; (c) two 2D hexagonally packed layers of micelles (AB); and (d) three layers with ABC (or FCC) stacking sequence structure. Figures (b–d) correspond to the radial geometry.

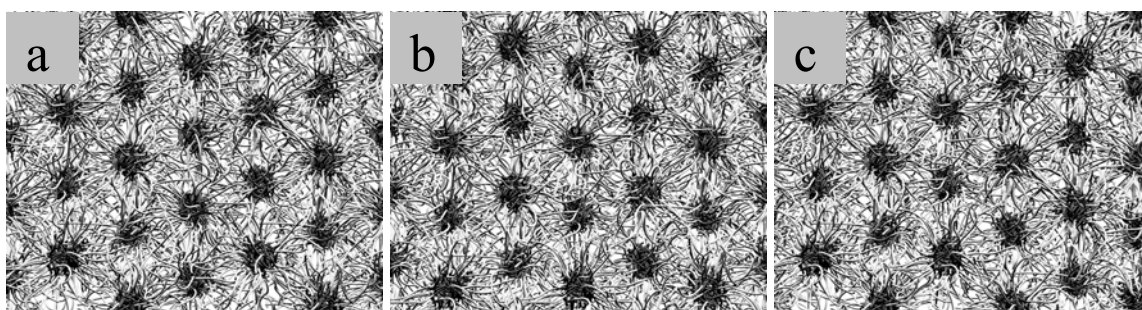


Figure 3.2 Tangential views of (a) ABC stacking sequence or FCC structure; (b) ABA stacking sequence or 3D hexagonal structure; and (c) Random AB stacking sequence.

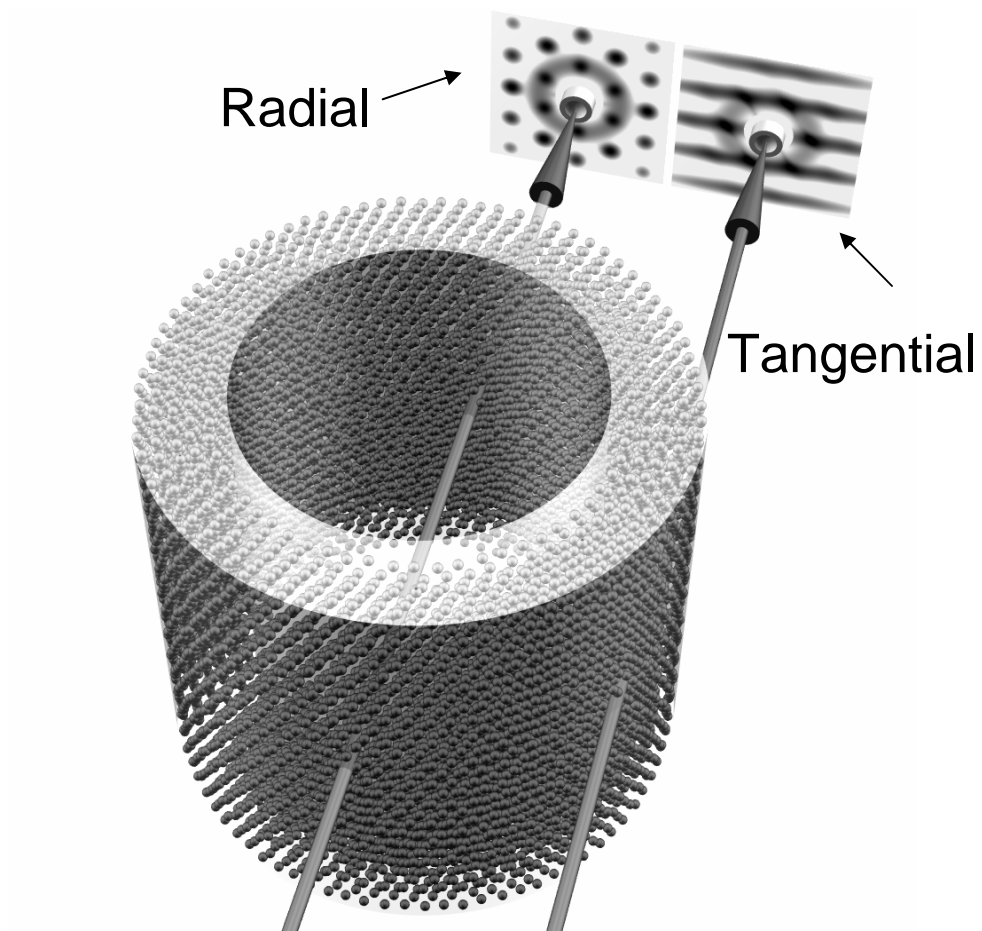


Figure 3.3 Configuration of the Couette cylinder used for the SANS measurements.

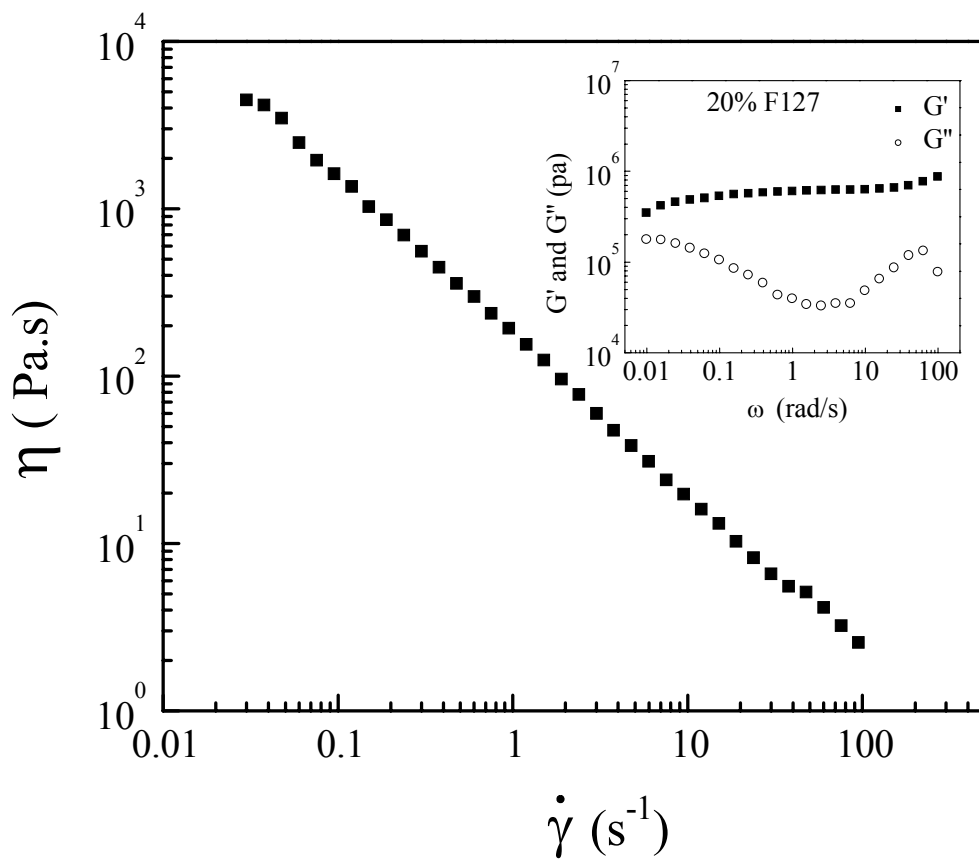


Figure 3.4 Steady shear viscosity η , as a function of the shear rate $\dot{\gamma}$, on a micelle gel of 20% Pluronic F127 in D_2O .

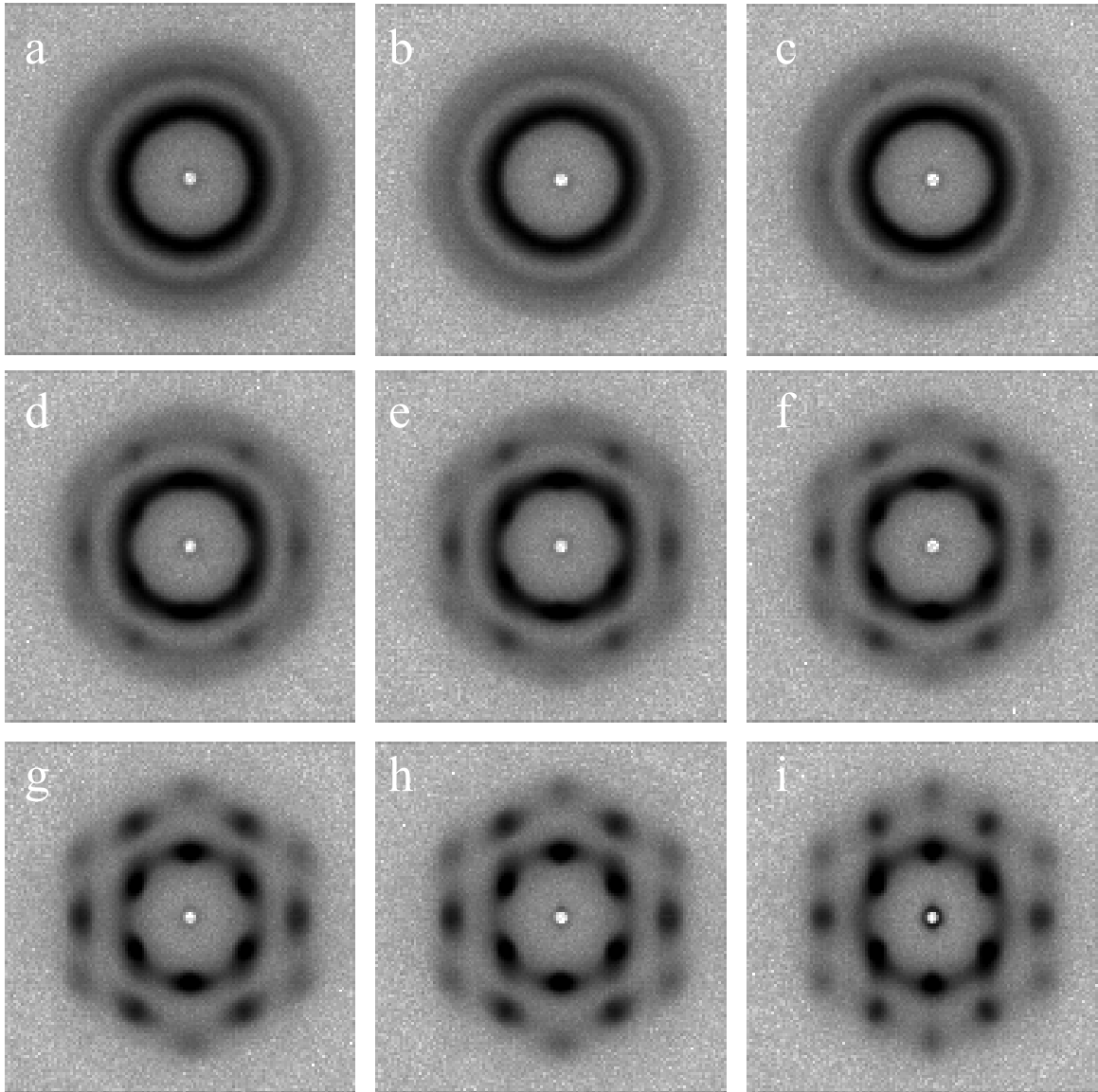


Figure 3.5 SANS radial scattering patterns from a to i for a 20% Pluronic F127 gel as a function of the shear rate: 0, 0.01, 1, 5, 10, 15, 30, 50 and 600 1/s.

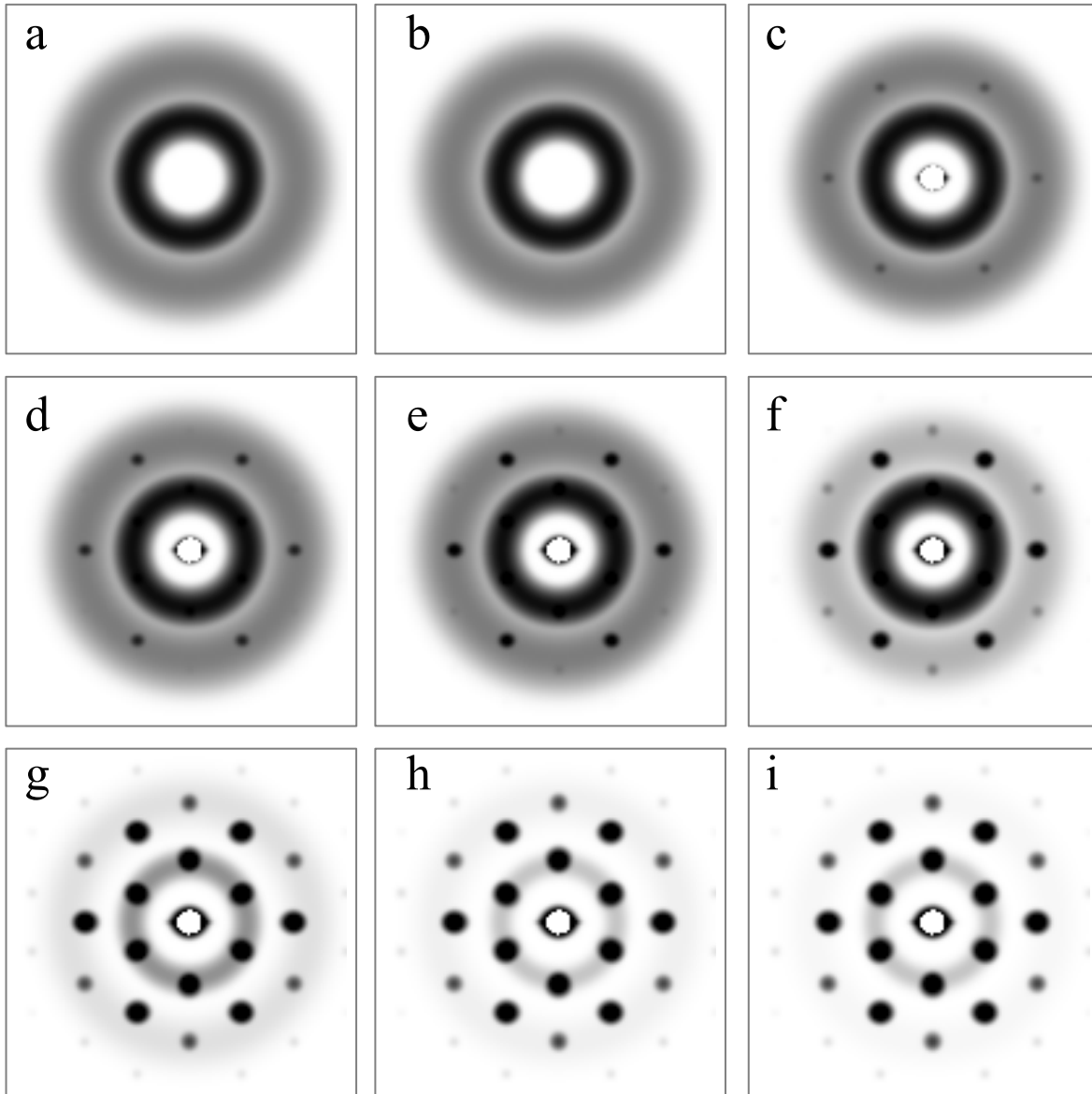


Figure 3.6 Calculated radial scattering patterns from a to i for a 20% Pluronic F127 gel, adapted for the experimental SANS patterns of Figure 5.

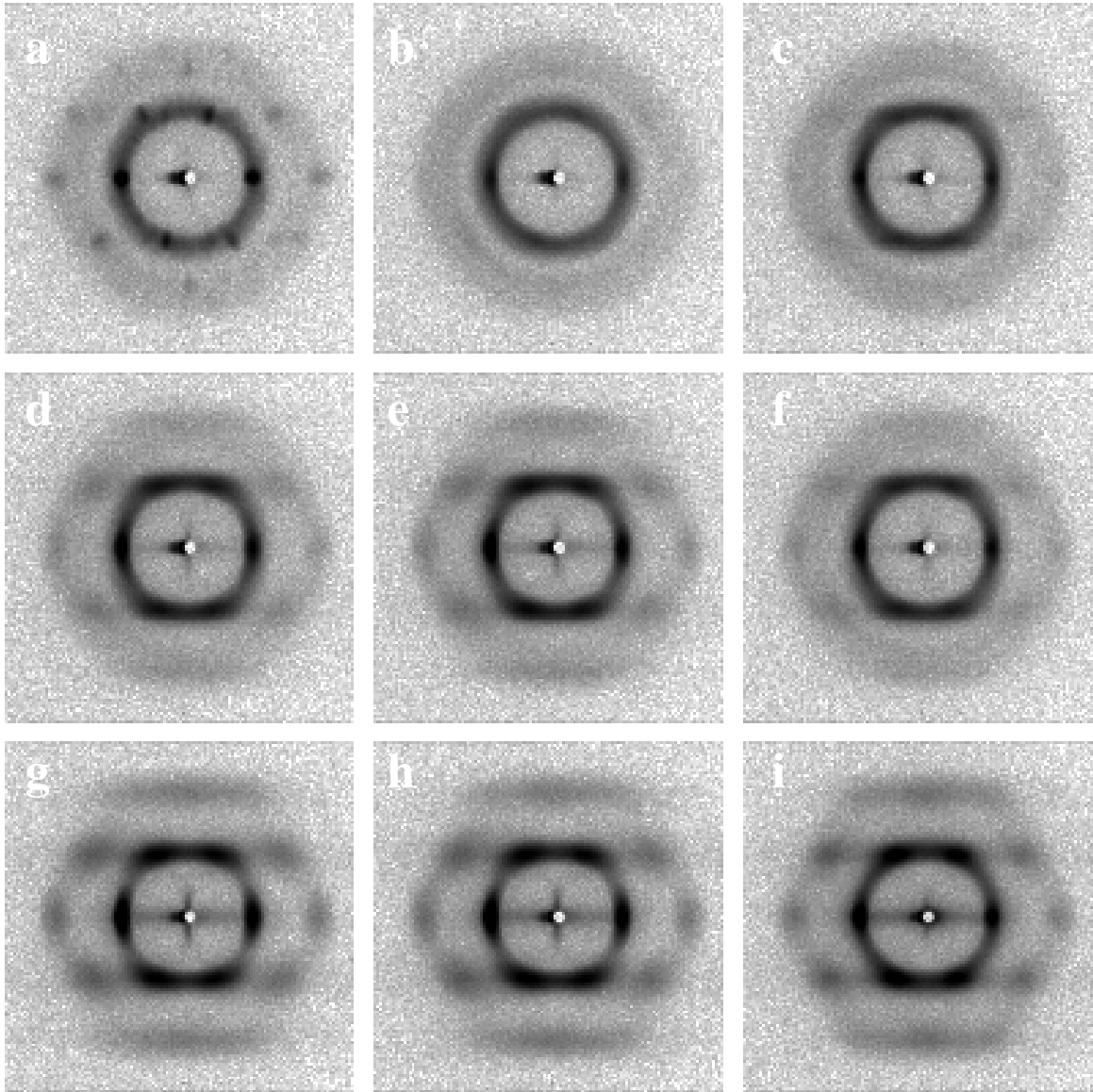


Figure 3.7 SANS tangential scattering patterns from a to i for a 20% Pluronic F127 gel as a function of the shear rate: 0, 0.01, 1, 5, 10, 15, 30, 50 and 600 1/s.

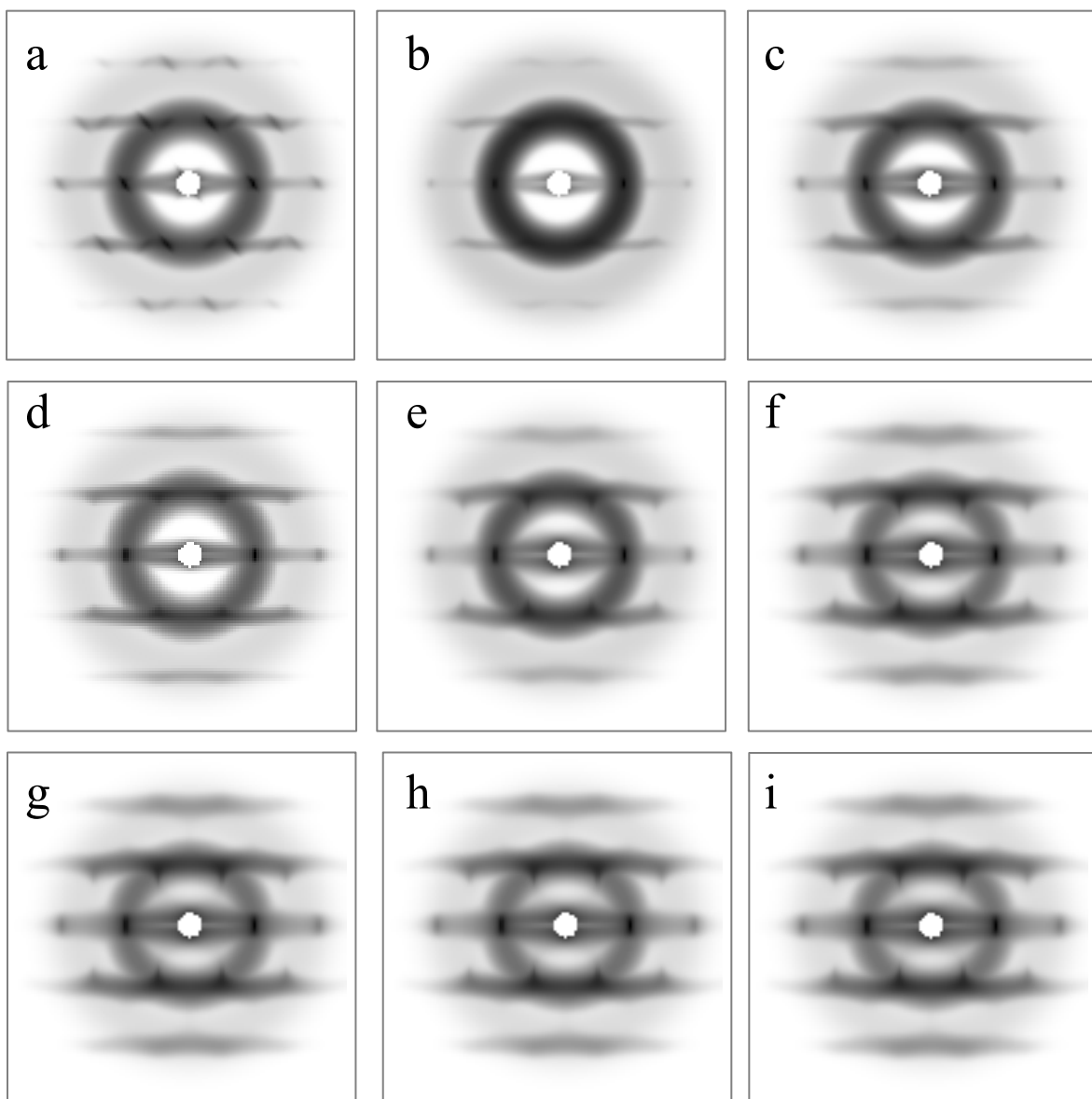


Figure 3.8 Calculated tangential scattering patterns from a to i for a 20% Pluronic F127 gel, adapted for the experimental SANS patterns of Figure 7.

CHAPTER 4

Rheology of Thermoreversible Hydrogels from Multiblock

Associating Polymers

(Submitted to Macromolecules 2007)

4.1 Introduction

Non-ionic amphiphilic triblock copolymers of poly(ethylene oxide)₉₉ - poly(propylene oxide)₆₇ -poly(ethylene oxide)₉₉ (Pluronic F127, PEO₉₉-PPO₆₇-PEO₉₉) have attracted a great deal of attention due to their thermoreversible gel-like behavior [1-4]. Numerous studies have been performed using a battery of complementary techniques [5-8], to try to understand the structure property relations responsible for the formation of these “smart” gels. In general, both PPO and PEO are water soluble at low temperatures and hence the F127 copolymer chains are fully miscible in aqueous solution. As the temperature increases, the PPO block is no longer hydrated and becomes hydrophobic. As a result, when the concentration is larger than the critical micellization concentration (cmc) = 6.1 mg/mL [5,6], individual micelles begin to form with a PPO core and PEO corona. Combining small angle X-ray scattering (SAXS) and small angle neutron

scattering (SANS), Wu *et al* showed that the micelles had a mean radius 11 nm and an aggregation number of 60. When the block copolymer concentration was increased even further (>15%, $T \cong 30 \text{ }^\circ\text{C}$) the micelles spontaneously self assembled into a face centered cubic structure [7]. Prud'homme *et al* proposed that the ordered micelle structures were due to repulsive interactions among the close-packed spherical micelles [8]. The material therefore exhibits a gel-like rheological response, even though none of the components are physically or chemically cross-linked to each other. On the other hand, the lack of actual cross-links results in the F127 micelle gel having a very low yield strength as the micelle layers can easily slide past each other under shear [9]. Hence, the rheological and structural properties of F127 gels limit its applications in some fields, such as tissue engineering and implantation, which requires high elastic modulus and yield strain.

In order to improve the mechanical properties of the gel, while still maintaining the thermo-reversibility, we synthesized multiblock structures, where the F127 construct would be repeated several times. In this manner, physical interconnections between the micelles could occur as the multiblock copolymers formed interlocking loops and tails, thereby greatly increasing the mechanical strength of the gels. Furthermore, by adding even a small amount of the multiblock to the F127 gels, we propose a model where a large enhancement of the mechanical properties could occur, as the longer chains could span more than

one micelle. This allows a new class of thermoreversible gels to be made where the rheological properties can be tailored to specific applications.

4.2 Experimental Section

Pluronic F127 (12,600 Daltons, 70% w/w PEO) was obtained from BASF (Mount Olive, NJ, USA). Gel permeation chromatography (GPC) measurements indicated that the Pluronic F127 had a polydispersity index of $M_w/M_n \sim 1.4$. The deionized water came from a Millipore-Q water purification system. HDI and the stannous 2-ethyl-hexanoate (SnOct_2) catalyst, were purchased from Aldrich and Sigma, respectively, and were used as received. The multiblocks were synthesized according to the procedures developed by Cohn *et al* [10], where identical units of F127 are linked together. A list of the polymers used is presented in Table 4.1. The multiblock copolymers generated have the following general structure: $[-\text{F127-HDI}]_p$, where p denotes the degree of polymerization, as shown in Figure 4.1. GPC data indicated that the molecular weight increased from 12,600 for the native F127, up to 58,000, for a material with $p = 4.6$. This polymer is denoted by PF 4.6. A variety of similar multiblocks were synthesized and their GPC molecular weights and polydispersity indices are listed in Table 4.1.

The gels were prepared by dissolving various amounts of the different polymers in deionized water which was stirred in an ice water mixture at $\sim 2^\circ\text{C}$

for 2 hours. These solutions were then refrigerated at 4 °C for 1–2 days to ensure that all the polymers were fully dissolved.

A Mettler Toledo DSC821 scanning calorimeter was used to study the heat capacity of solutions as a function of temperature. Typically 6–12 mg solutions were placed in aluminum pans, which were then carefully sealed. The scans were carried out in a dry nitrogen environment at a constant heating rate of 1 °C /min between 2 and 50 °C, with an empty aluminum pan as reference.

To measure the structure of the Pluronic F127 and the multiblock copolymer gels, SANS experiments were performed at the National Institute of Standards and Technology reactor division. Data were collected on an area sensitive detector at the NG3 (NIST/Exxon/U.Minn) SANS Beamline, with sample to detector distance of 3.45 m. The nominal wavelength of the neutrons was 6.00 Å with a dispersity $\Delta\lambda/\lambda$ of 0.10 and an average incident intensity of approximately 464,500 neutrons/s. The accessible range in $q \equiv (4\pi/\lambda)\sin(\theta/2) = 0.0055$ to 0.1858 \AA^{-1} , where θ is the angle between incident and scattered beam. The samples were placed inside a sample holder with a width of 5 mm. Samples were loaded carefully at 2 °C to minimize the shear effects, and then temperature was increased to 37 °C and stabilized for 20 min.

Rheological measurements of polymer gels were performed on a strain-controlled rheometer, Rheometrics Fluids Spectrometer II (RSF II), using concentric cylinders, with an inner diameter of 16.5 mm, an outer diameter of

17.1 mm and 13.7 mm height. Temperature control was achieved using a water bath surrounding the outer cylinder. The concentric cylinder geometry was loaded with the polymer solutions at 2 °C (liquid state). Temperature sweep measurements were performed at a constant heating rate of 1 °C/min. Low viscosity silicone oil was added to the surface of the sample to minimize evaporation of water.

The instrument was used in the oscillatory mode, in which the outer cylinder is rotated sinusoidally at a given frequency. The frequency dependence of the complex modulus was determined between 0.01 and 100 rad/s. The sol-gel transition temperature of polymer gels was determined from an oscillatory shear temperature sweep at 1 rad/s. The sol-gel transition temperature was measured for all the gels, operationally defined here as the temperature at which the storage modulus G' was half of the largest value for the high-temperature gel [11].

4.3 Results

Differential Scanning Calorimetry. DSC measurements were carried out on F127 and multiblock copolymer solutions. The results are shown in Figure 4.2 where we see that a large endothermic peak occurs, at the same position, $T \cong 12$ °C, for all the Pluronic gels, which has been shown to arise from the desolvation of the PPO groups [12]. The peak is broader for the multiblock copolymers than

for the pure F127 copolymer, indicating that the desolvation process may be partially hindered by the block structure. A second small peak is also apparent for the F127 polymer at $T \cong 20$ °C, which was previously attributed to the transition from isotropic to cubic packing of micelles [12]. This small peak is not observed for the multiblock copolymer systems, either due to resolution broadening or implying that they do not form ordered cubic structures. This latter conclusion was supported by the SANS data, as shown below.

SANS. In order to determine the micelle structure of the copolymers, we performed small angle neutron scattering. The scattering at small angles is usually attributed to the Bragg diffraction caused by interparticle interference, while the scattering at larger angles is recognized as intraparticle scattering. Figure 4.3 reveals the F127 and the PF polymers have the same peak at low q , which means they have the same d spacing distance between micelles, or $d \cong 17.2$ nm. The second set of peaks, which are clearly resolved in the F127 copolymer, but overlapping for the multiblock structure, indicate that the micelles adopt an FCC structure when gelation occurs [7]. The second peak is actually a doublet corresponding to the (220) and (311) plane reflections, which are barely resolved for the F127 polymer, but nonexistent for the multiblocks, indicating significantly less long-range order in the multiblocks.

In Figure 4.4 we show the SANS scattering patterns from 20% solutions of F127 (4.4a), PF4.6 (4.4b) and a mixture containing 2% multiblock, and 18% F127

(4.4c) at rest (leftmost) and at shear rates of 1 s^{-1} , 10 s^{-1} and 100 s^{-1} moving from left to right. From the figures we can clearly see that the F127 becomes increasingly ordered with shear. On the other hand, the pure multiblock systems become increasingly disordered with increasing shear. The structure for F127 underwent a transition from a face center cubic (FCC) lattice to a two-dimensional hexagonal close packing (HCP) layered structure under steady shear [9]. However, in Figures 4.4b and 4.4c, we found that no layered structure formed for any of the multiblock gels. In fact the ring nearly disappears altogether for the multiblocks. In ref 9 the alignment was described as planes of micelles that slide across each other under steady shear. Gliding planes are not possible unless bridges stay within a plane. It is interesting to note that in the mixture of the two gels, the behavior under shear is much closer to that of the multiblock than to the response of the single block structure, again indicating that even a small amount of interconnected micelles was sufficient to destroy the long range order previously observed for F127 FCC gels [7,9].

Rheology. The rheological behavior of the multiblock copolymers was measured as a function of concentration and degree of polymerization and the results were compared to that of the F127 triblock copolymer at the same total copolymer concentration. Figure 4.5 compares linear viscoelastic data in the form of frequency sweeps at $37 \text{ }^\circ\text{C}$ for 20% PF 3.2 and 20% F127 (inset). The two samples exhibit similar storage modulus but the PF 3.2 gel shows more relaxation

(higher loss modulus and stronger frequency dependence of storage modulus) in the rubbery plateau, owing to its less perfect structure. In contrast, the FCC structure of the F127 gel has $\tan \delta \equiv G''/G' < 0.1$ in the midst of the rubbery plateau, suggesting minimal relaxations in F127 for $1 < \omega < 5$ rad/s.

Figure 4.6 reports strain sweep data for 20% F127, 20% PF 3.2 and 20% PF 4.6 at 1 rad/s and 37 °C. The F127 gel begins to yield starting at very low strain (0.01), consistent with the sliding plane model proposed from analysis of the SANS data [9]. As long as the planes are not physically connected they can easily slide past each other. An abrupt change can be seen in the response of all copolymers with degree of polymerization exceeding three. These materials have slightly higher modulus than the F127 gel but twenty times larger yield strain (0.2). The considerably larger yield strain is consistent with the expected structure, with multiblock chains spanning (and connecting) several micelles in different layers. To focus on the linear response, we utilize a strain amplitude of 0.001 in what follows.

PF Multiblock gel: Figure 4.7 presents temperature sweeps at 1 rad/s for different concentrations of PF 3.2, showing that the storage modulus (G') increases with concentration and rapidly increases with temperature, near the gel point, for all concentrations greater than 5%. In Figure 4.8 we plot the gel point temperature, T_{gel} and the largest value of G' for $T > T_{\text{gel}}$, as a function of PF 3.2 concentration. This gel modulus increases by more than three orders of magnitude

when the concentration of polymer is increased from 5 to 10%. The modulus continues to increase with concentration above 10%, but at a much slower rate. Hence, the primary difference between the F127 copolymer and the PF 3.2 multiblock copolymer is the concentration needed for the onset of gelation: 15% for F127 and slightly below 10% for PF 3.2.

The inset of Fig. 4.8 shows that the gelation temperature of PF 3.2 has a similar concentration dependence to that observed for F127 [13]. The temperature dependence of the storage modulus at $\omega = 1 \text{ s}^{-1}$ for copolymers with different degree of polymerization at a fixed concentration of 20% is shown in Figure 4.9. The gelation temperature seems to be fairly independent of the degree of polymerization (for $\text{PF} > 3$), consistent with the assumption that the gelation temperature is simply due to desolvation of the PPO block. The maximum of the temperature dependence of G' (1 s^{-1}) for each sample in Fig. 4.9, increases with degree of polymerization but rapidly saturates, as shown in Figure 4.10. The largest difference occurs between a degree of polymerization of 1 (pure F127) and a degree of polymerization of 2.5. No significant increase occurs for larger block copolymer numbers. These results indicate that the multiblock rheological behavior is due to formation of a reversible physical gel, or a network of interconnected micelles at high concentration.

Mixtures of F127 and PF multiblock copolymer: In order to determine whether the addition of PF multiblock copolymer could enhance the viscoelastic

response of the F127 gel, we measured the storage modulus of F127 gels mixed with PF 4.6. In Figure 4.11 we plot elastic modulus G' of a gel composed of a total of 25% by weight polymer, consisting of a mixture of F127 and PF 4.6 copolymer. G' increases sharply as PF multiblock is added, eventually leveling off at a value an order of magnitude higher than that of the pure F127 sample at the same concentration. It is interesting to note that at an overall concentration of 25%, the F127 solution is far above the micelle gel concentration. Yet, despite the relatively low concentration of multiblock, it is effective in raising the modulus by nearly an order of magnitude.


A much more dramatic effect can be seen when the multiblock copolymer is added to an F127 solution just below its gelation concentration of 15%. In Figure 4.12 we show the temperature dependence of the storage modulus of F127 mixed with varying amounts of PF 4.6, where the total polymer concentration is fixed at 14.5%. The 14.5% solution of F127 is liquid-like at all temperatures. Addition of 4.83% PF 4.6 multiblock increases the modulus by nearly three orders of magnitude, at 40 °C, indicating that the gel has already formed. From percolation theory [14], we know that the modulus of a system close to its gel point is written as a power law in the proximity to the gel point. We apply these percolation ideas to the concentration of multiblock c and the concentration of multiblock corresponding to the gel point c_{gel} .

$$G \sim \left(\frac{c - c_{gel}}{c_{gel}} \right)^{\beta+1/\sigma} \quad (1)$$

For a three-dimensional percolation, the exponents $\beta = 0.41$ and $\sigma = 0.45$, making $\beta + 1/\sigma = 2.6$. In Figure 4.13, we plot $(G'_{max})^{0.38}$ as a function of concentration for the different multiblocks where we can see that a good fit is obtained without any other free parameters, indicating that percolation theory is applicable to this system. (0.38 is $1/(\beta + 1/\sigma)$) This is in contrast to the pure F127 solutions, known to be composed of unconnected micelles, forming a FCC crystal of micelles [7,9]. Addition of the multiblocks physically connects the isolated micelles, hence the ordering into the FCC lattice which occurs at higher concentration is no longer needed to form a physical gel.

In order to estimate the percolation concentration c_{gel} for each multiblock, we note the concentration at which the steepest straight lines in Figure 4.13 extrapolate to a modulus of zero. These gel concentrations are all close to $c_{gel} = 1\%$ multiblock, apparently independent of the degree of polymerization of the multiblocks.

4.4 Discussion

 the absence of multiblock copolymer, SAXS data [7] indicate that the polymer solution of 14.5% is far above the critical micellization concentration

(CMC), and the F127 polymer exists in the form of micelles ~ 20 nm in diameter. When the F127 concentrations are above the critical gelation concentration ($\sim 15\%$), the gels spontaneously order into an FCC structure of close packed micelles, which obstructs flow and increases the viscosity. Since the F127 micelles are not physically connected, this structure yields easily in shear and at a shear rate of 0.01 s^{-1} , planes of micelles slide past each other [9].

At the concentration of 14.5%, SANS data indicate no long range order in the F127 solution [9]. From the rheological data on the pure multiblock solutions, we know that a physical gel forms, at a critical concentration of slightly below 10%. Therefore when we only add a small amount of the multiblock copolymer to the F127 solutions, we can assume that there is insufficient copolymer to form the FCC structure of close packed micelles. Rather, the copolymer chains, may become incorporated into the F127 micelles, as shown in Figure 4.14. The multiblocks can form bridges between micelles (Fig. 4.14b) resulting in physical crosslinks between the micelles.

Figure 4.13 suggests that the percolation concentration is $c_{gel} = 1\%$ multiblock. Knowing the F127 concentration and the aggregation number of F127 micelle [7], $N=60$, and coordination number of the micelles, we estimate that $c_{gel} = 1\%$ multiblock corresponds to 0.966 multiblock chains per micelle for 1% PF 4.6 in 13.5% F127 solutions with overall concentration 14.5%. The number of 0.966

suggests that each PF 4.6 chain contributes on average one intermicelle crosslink, as the gel point corresponds to one crosslink per structural unit [14].

4.5 Conclusion

Multiblock copolymers of poly(ethylene oxide)₉₉-poly(propylene oxide)₆₇-poly(ethylene oxide)₉₉ were synthesized by chain extending with hexamethylene diisocyanate (HDI). The resulting multiblock copolymer P[F127]_p maintained the thermoreversible properties of the original F127 triblock unit. The rheological and structural properties of the gel were characterized as a function of temperature, composition and degree of polymerization. Mixtures of multiblock and F127 copolymers were also studied. Using neutron scattering we found that a large degree of alignment could be induced in the F127 gel [9], but no long-range order could be found in the gels formed in multiblock solutions or in the F127/multiblock mixed solutions. The yield strain in samples with polymers consisting of 3.2 or more blocks was nearly an order of magnitude higher than the F127 gel, possibly making these multiblocks and/or their mixtures with F127 useful for biomedical applications. For F127 solutions slightly below the concentration needed to form a gel, substitution of F127 with multiblocks at constant overall concentration forms a gel, with modulus described by percolation theory, as each multiblock apparently bridges two F127 micelles.

4.6 References

- [1] Xiong, X. Y.; Tam, K. C.; Gan, L. H. *Journal of Nanoscience and Nanotechnology* **2006**, 6, 2638–2650.
- [2] Chun, K. W.; Lee, J. B.; Kim, S. H.; Park, T. G. *Biomaterials* **2005**, 26, 3319–3326.
- [3] Higuchi, A.; Yamamoto, T.; Sugiyama, K.; Hayashi, S.; Tak, T. M.; Nakagawa, T. *Biomacromolecules* **2005**, 6, 691–696.
- [4] Cohn, D.; Sosnik, A.; Garty, S. *Biomacromolecules* **2005**, 6, 1168–1175.
- [5] Mortensen, K.; Talmon, Y. *Macromolecules* **1995**, 28, 8829–8834.
- [6] Alexandridis, P.; Holzwarth, J. F.; Hatton, T. A. *Macromolecules* **1994**, 27, 2414–2425.
- [7] Wu, C.; Liu, T.; Chu, B.; Schneider, K. D.; Graziano, V. *Macromolecules* **1997**, 30, 4574–4583.
- [8] Prud'homme, R. K.; Wu, G.; Schneider D. K. *Langmuir* **1996**, 12, 4651–4659.
- [9] Jiang, J.; Burger, C.; Li, C.; Lin, M. Y.; Rafailovich, M. H.; Sokolov, J. C. *Macromolecules* **2007**, 40, 4016–4012.
- [10] Cohn, D.; Sosnik, A.; Levy, A. *Biomaterials* **2003**, 24, 3707–3714.
- [11] Edsman, K.; Carlfors, J.; Peterson, R. *Eur. J. Pharm. Sci.* **1998**, 6, 105–112.
- [12] Wanka, G.; Hoffmann, H.; Ulbricht, W. *Macromolecules* **1994**, 27, 4145–4159.

[13] Ricci, E. J.; Bentley, M.; Farah, M.; Bretas, R.; Marchetti, J. M. *European Journal of Pharmaceutical Sciences* **2002**, 17, 161–167.

[14] Rubinstein, M.; Colby, R. H. *Polymer Physics*: Oxford University Press, New York, **2003**.

Table 4.1 Molecular Characteristics of Triblock F127 and the Multiblock Copolymers

Name	Degree of Polymerization* (<i>p</i>)	Molecular Weight (g/mole)	Polydispersity (Mw/Mn)
F127 \equiv PF1.0	1.0	12,600	1.40
PF1.9	1.9	23,900	1.63
PF2.5	2.5	31,500	1.67
PF3.2	3.2	40,300	1.46
PF4.6	4.6	58,000	1.85
PF5.6	5.6	70,600	2.08
PF6.0	6.0	75,600	1.44

* Degree of polymerization was calculated as the ratio of GPC molecular weight and that of the “monomeric” F127 (which we run with all samples as an internal standard).

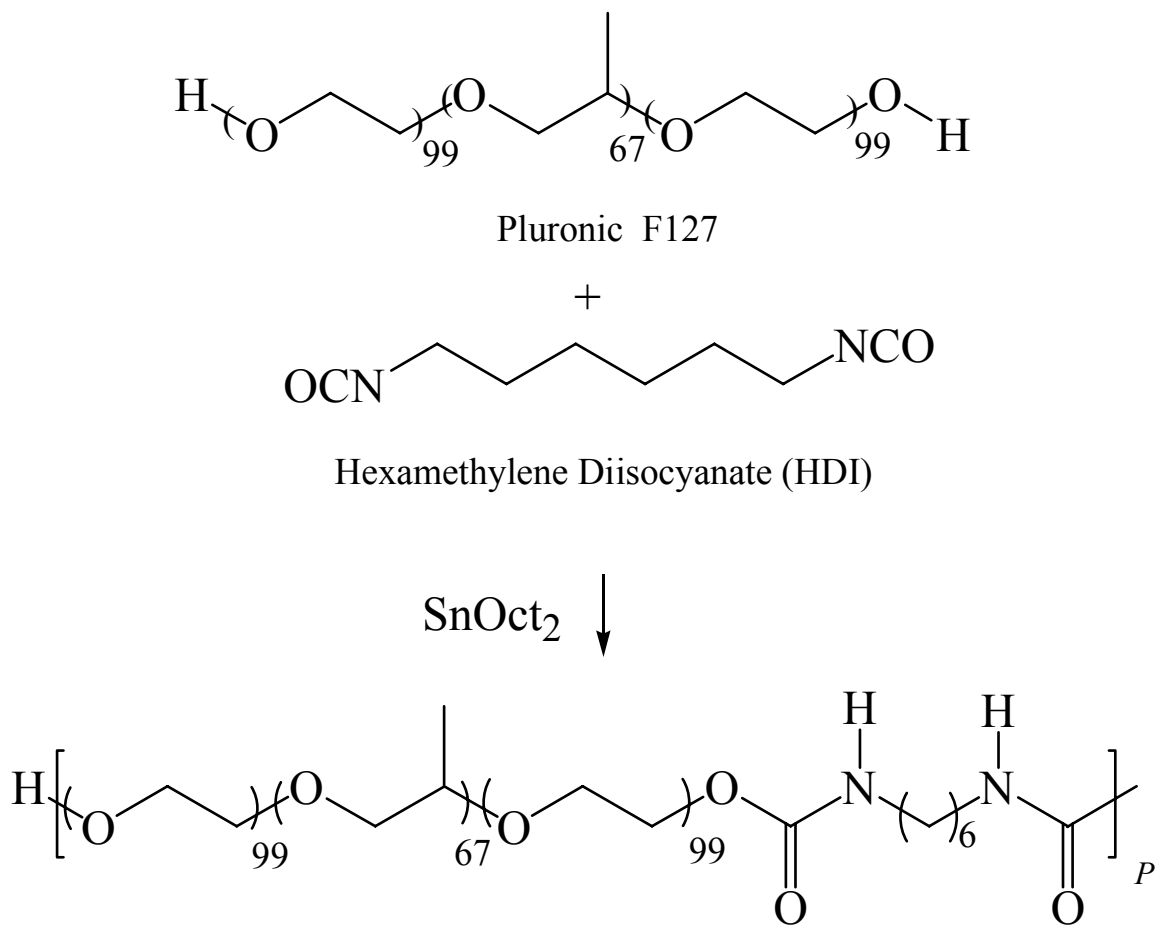


Figure 4.1 Chain extension of Pluronic F127 with hexamethylene diisocyanate.

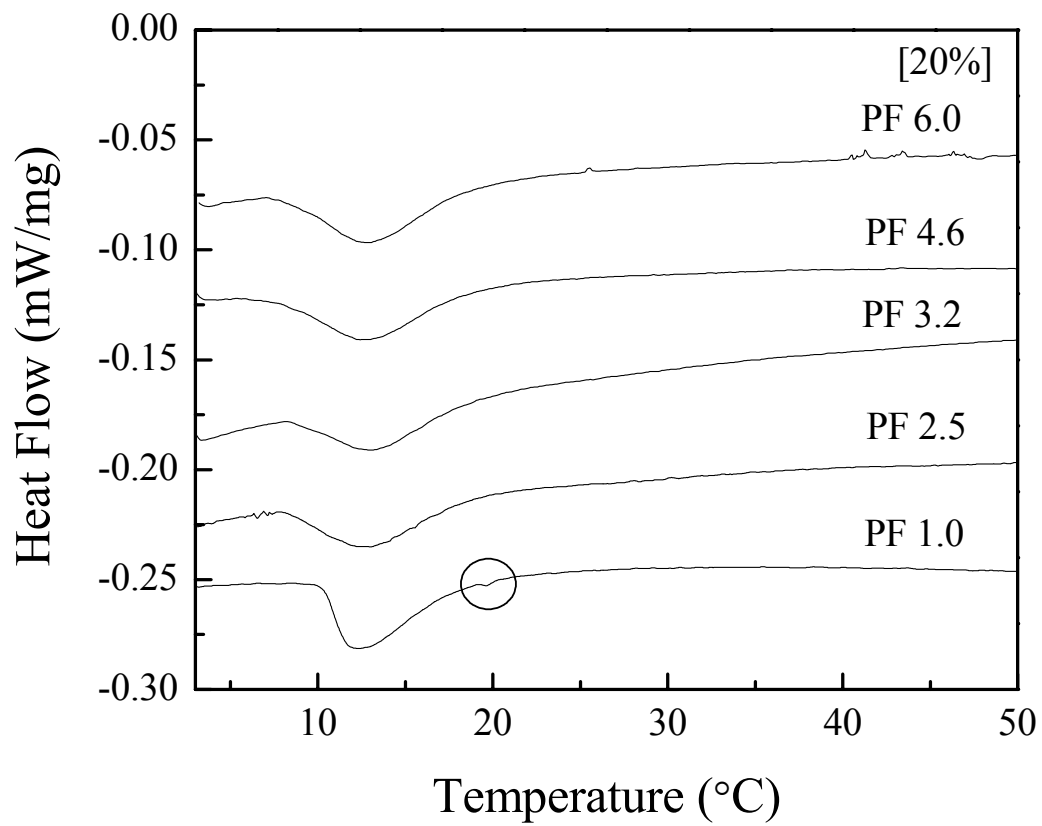


Figure 4.2 DSC measurements on the 20% solutions of different multiblock copolymer at 1 °C/min heating rate.

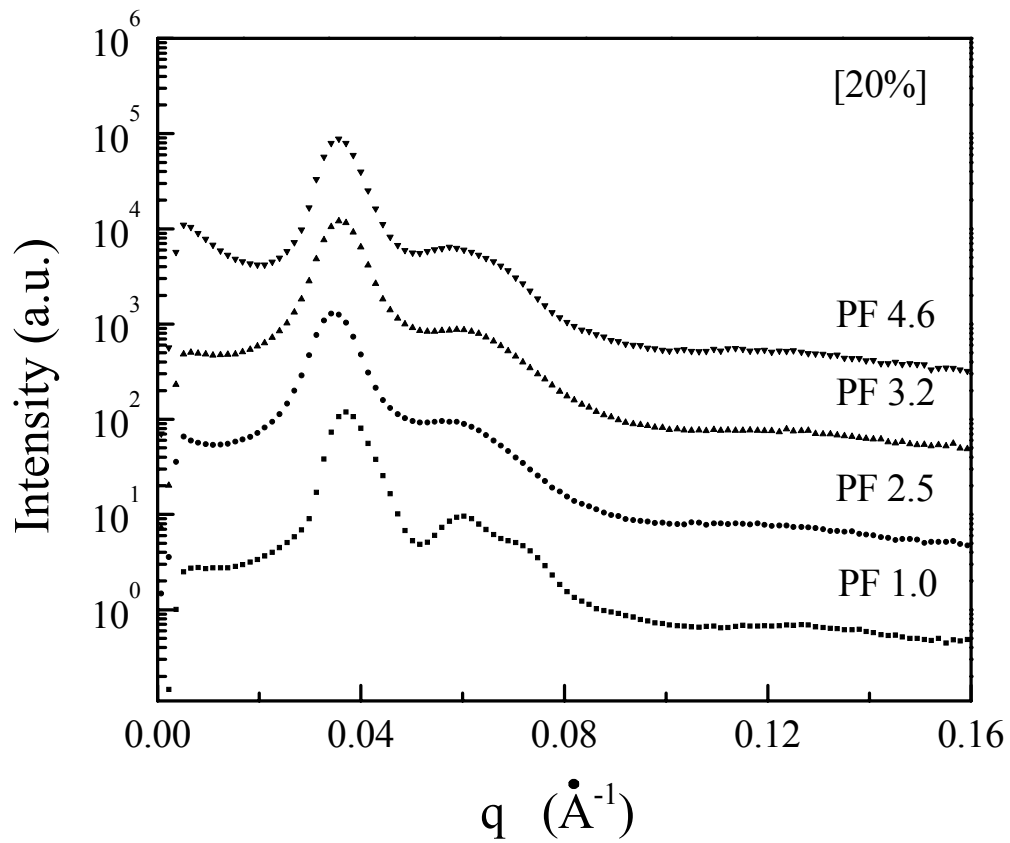
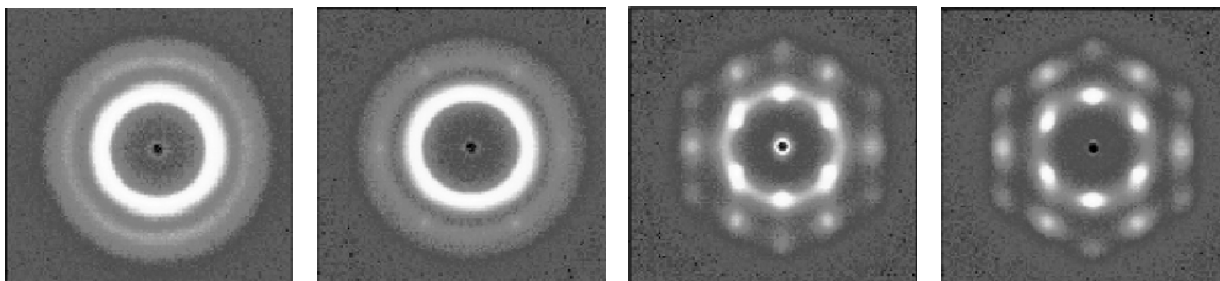
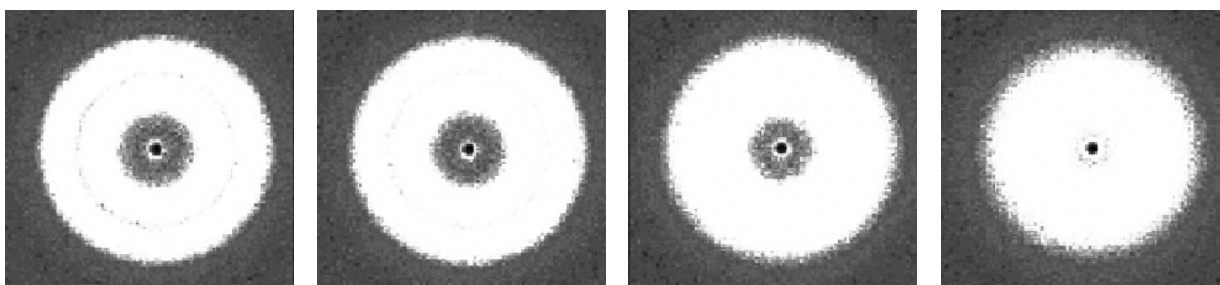


Figure 4.3 SANS scattering profiles of different PF copolymer gels at 37 °C at rest.

(a) 20% F127 gel



(b) 20% PF 4.6 gel



(c) Mixture of 18% F127 and 2% PF 4.6

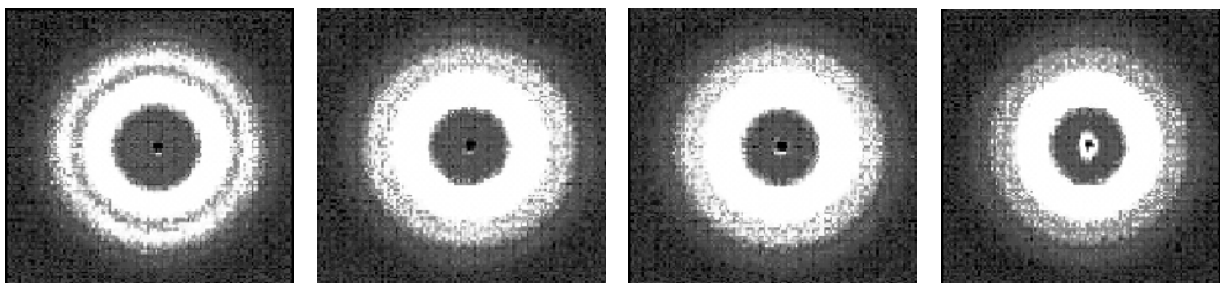


Figure 4.4 SANS scattering patterns for: (a) 20% F127 gel; (b) 20% PF 4.6 gel; and (c) Mixture of 18% F127 and 2% PF 4.6, with increasing the shear rate 0, 1, 10 and 100 1/s. Shear direction is perpendicular to the beam direction.

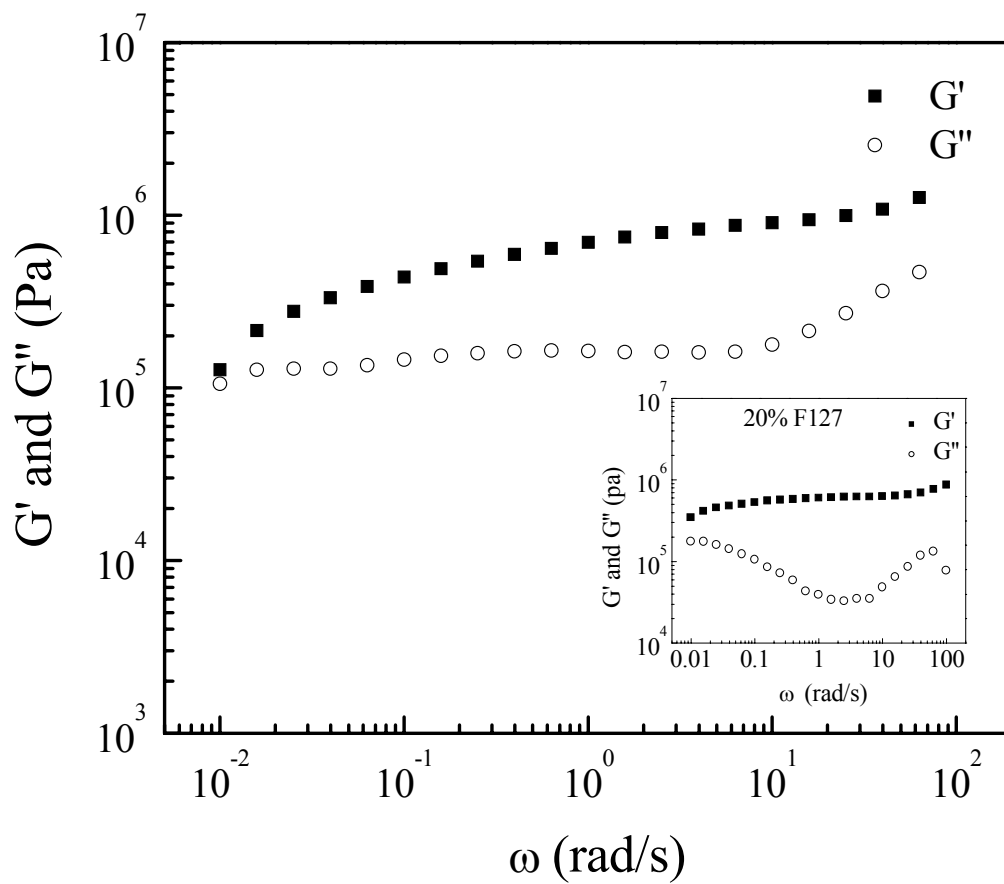


Figure 4.5 Frequency dependence of storage and loss modulus of 20% PF 3.2 and 20% F127 (inset) at a strain of 0.001 and 37 °C.

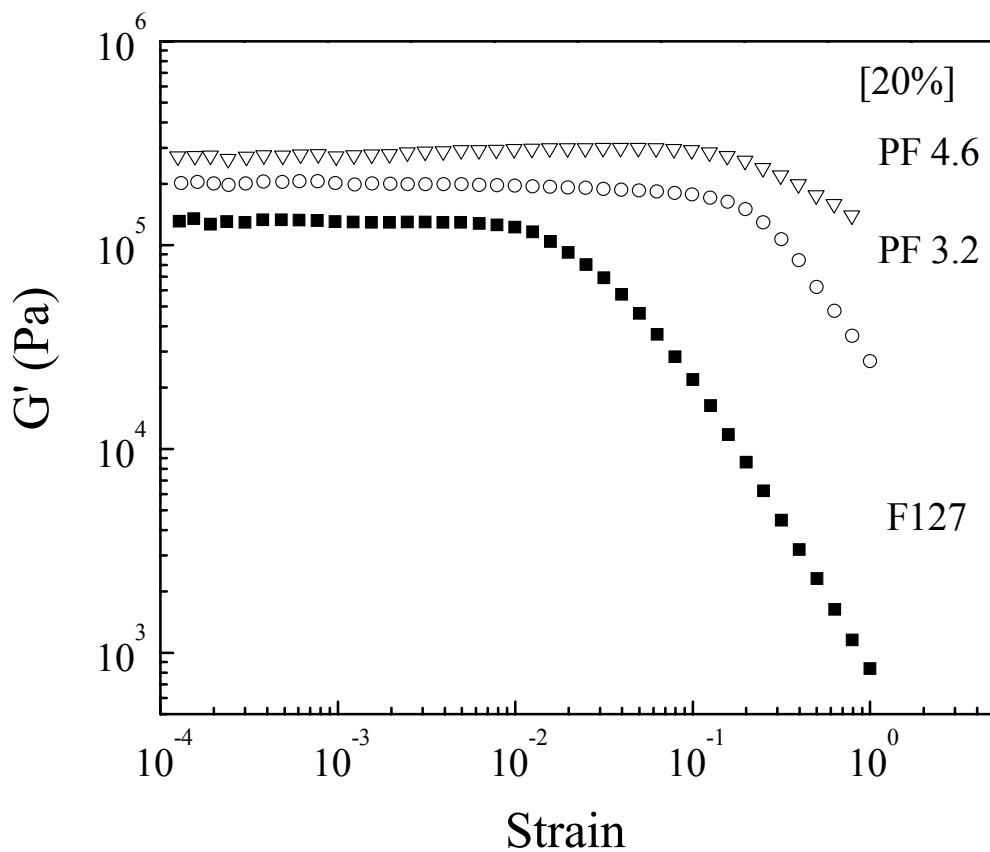


Figure 4.6 Storage modulus as a function of strain amplitude for 20% gels of F127 and different PF multiblock copolymers at a frequency 1 rad/s and 37 °C.

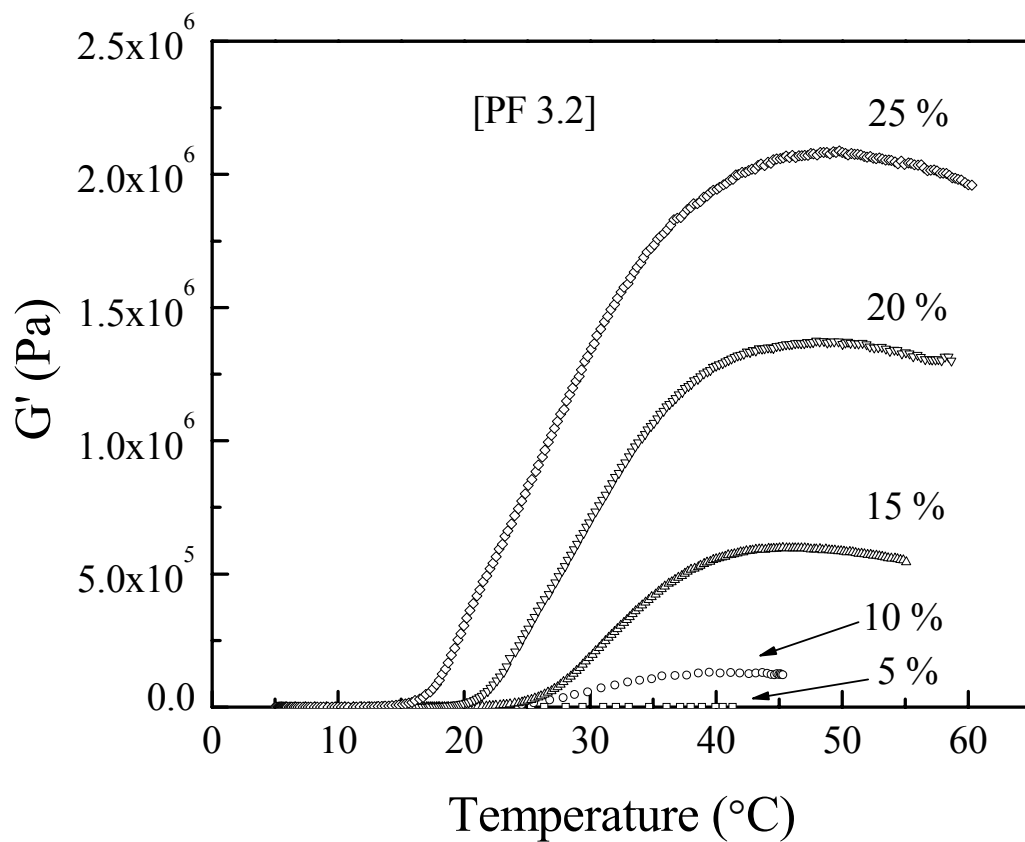


Figure 4.7 Storage modulus of different concentrations of PF 3.2 polymer gels during heating at 1 $^{\circ}\text{C}/\text{min}$ at a frequency of 1 rad/s and strain amplitude of 0.001.

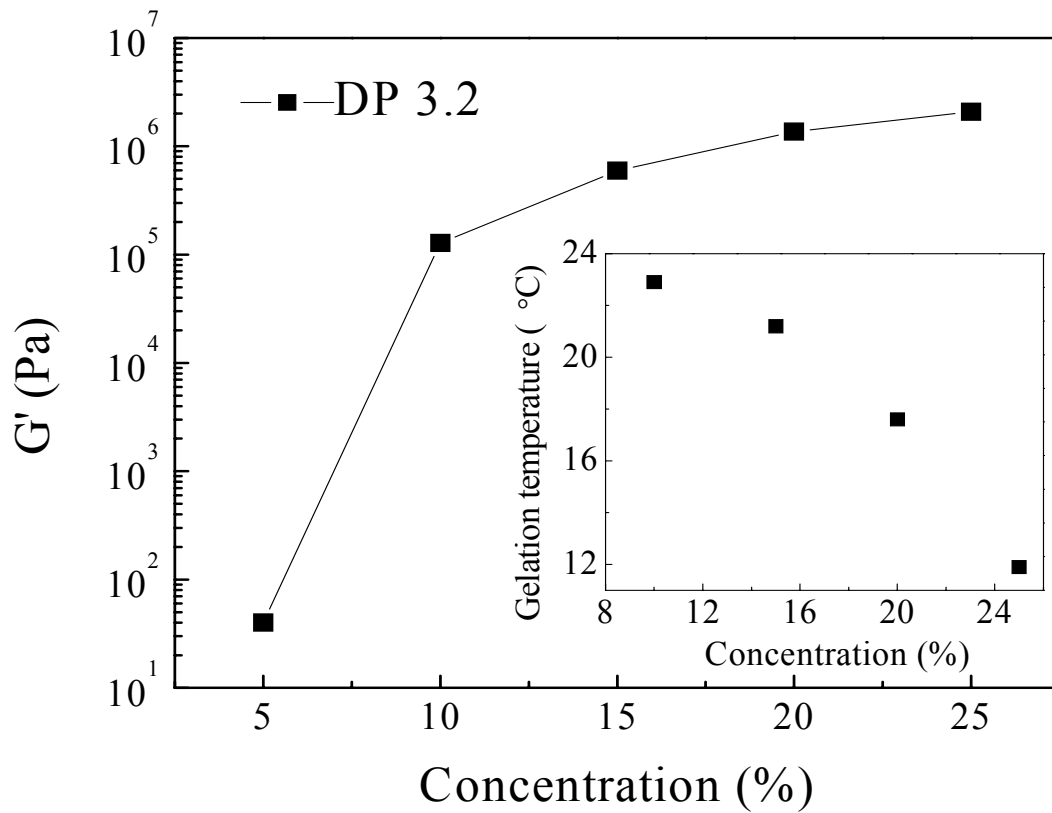


Figure 4.8 Storage modulus and gelation temperature (inset) of PF 3.2 gels as functions of concentration.

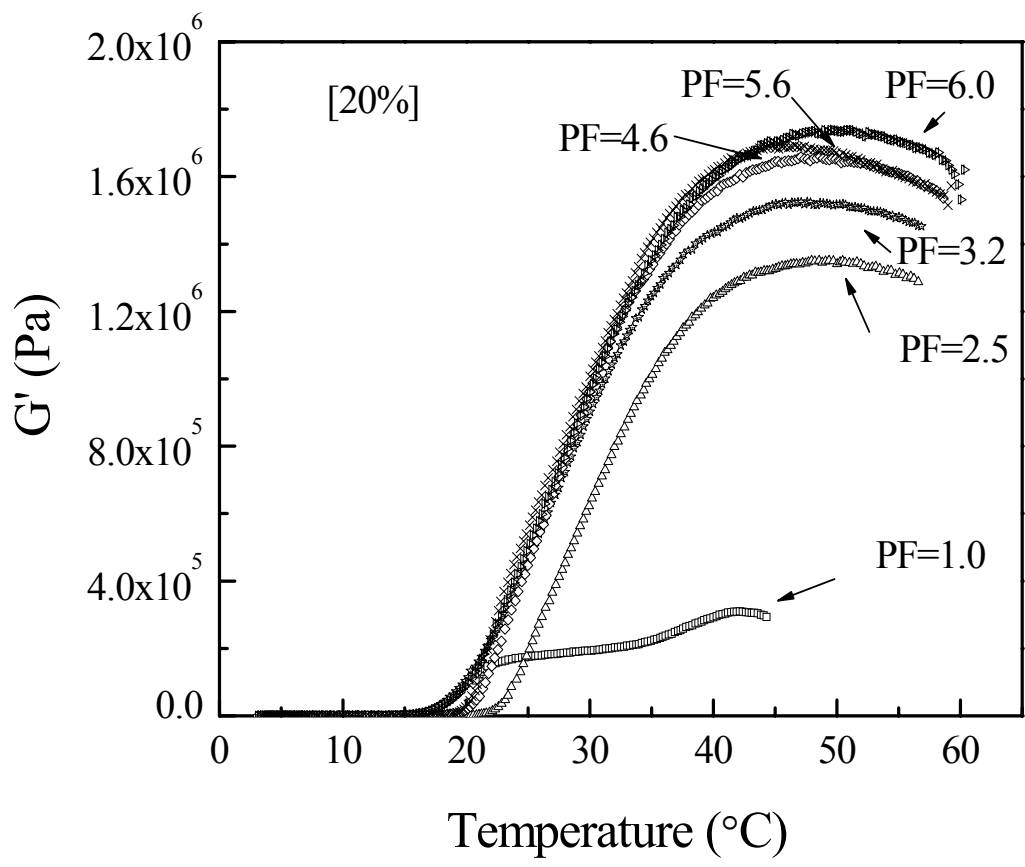


Figure 4.9 Storage modulus of 20% polymer gels during heating at $1^{\circ}\text{C}/\text{min}$ at a frequency of 1 rad/s and strain amplitude of 0.001 .

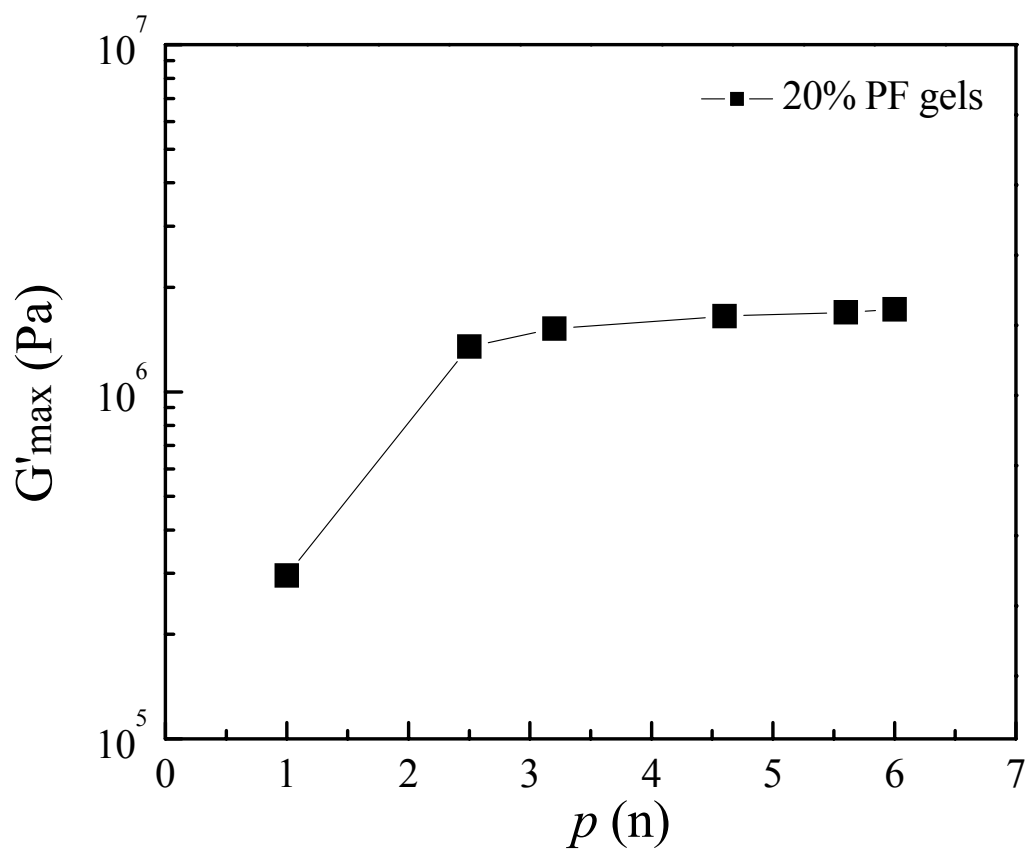


Figure 4.10 Storage modulus of 20% polymer gels as a function of degree of polymerization.

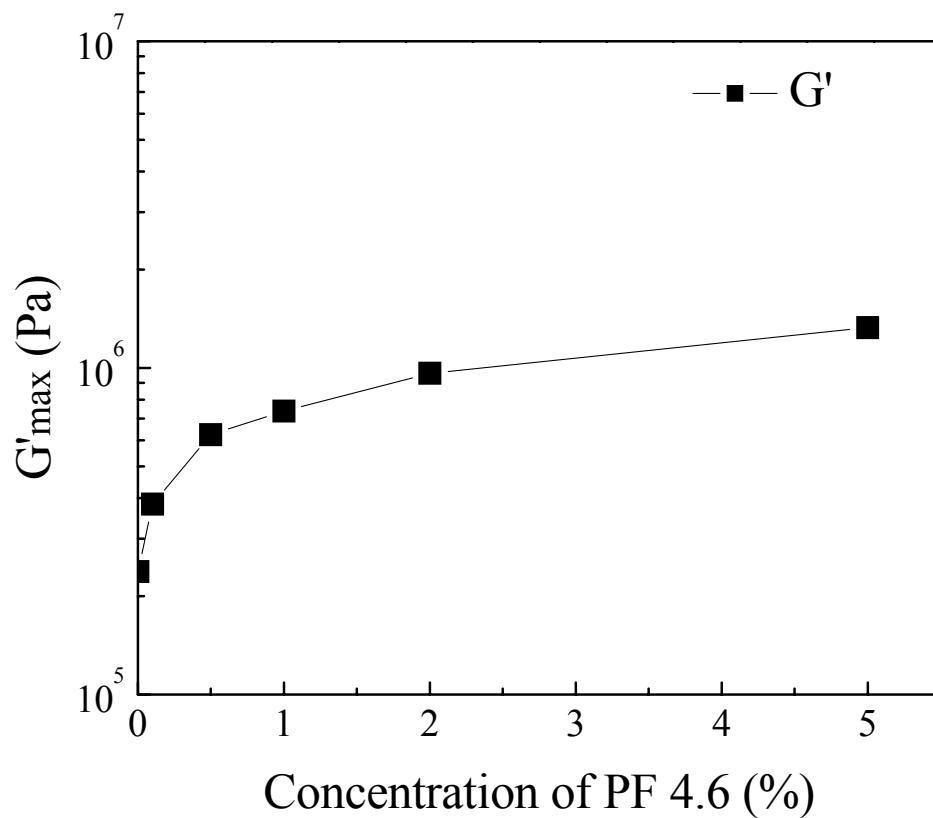


Figure 4.11 Storage modulus of 25% polymer gels of F127/PF 4.6 mixtures as a function of the concentration of PF multiblock copolymer.

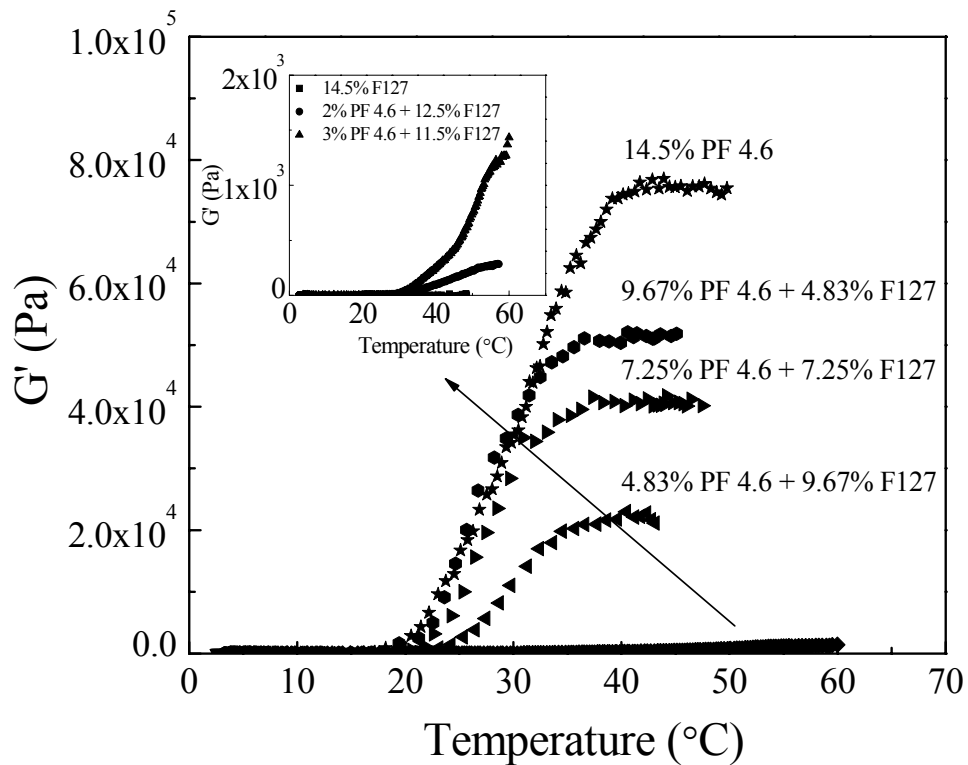


Figure 4.12 Storage modulus of F127 and F127/PF 4.6 mixtures, all with an overall concentration of 14.5%, during heating at 1 °C/min at a frequency of 1 rad/s and strain amplitude of 0.001. (The inset represents of the storage modulus of low PF 4.6 concentrations which is not distinguishable in the scale of original figure.)

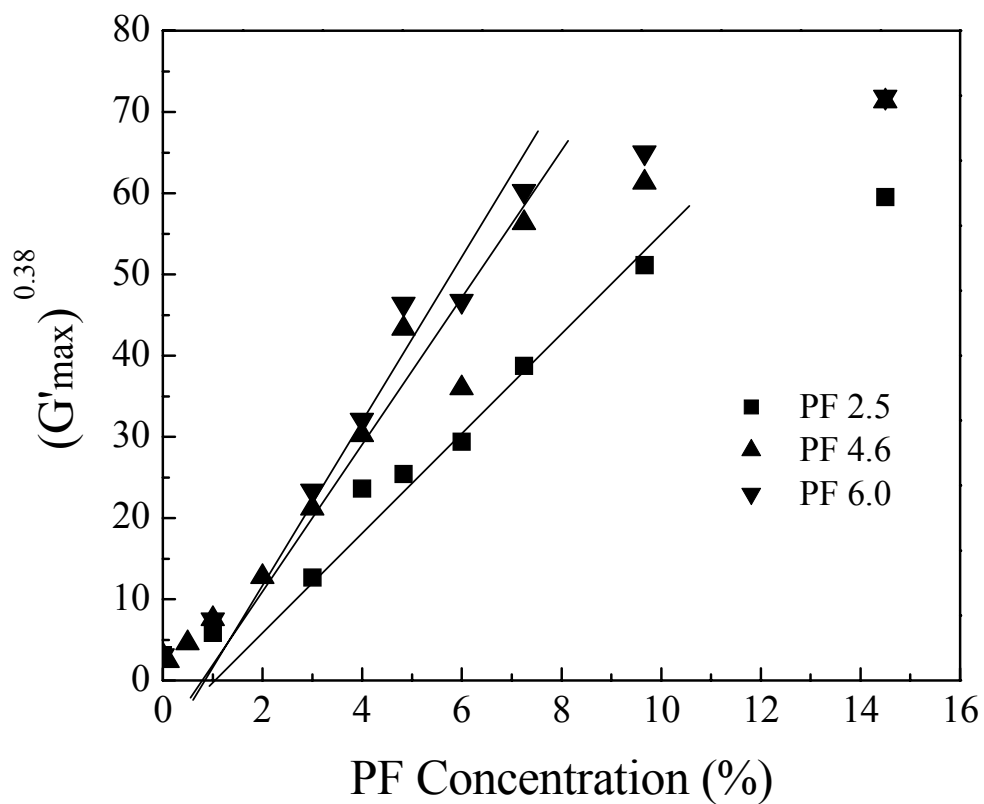


Figure 4.13 Maximum value of the (high temperature) storage modulus of gels made by mixing F127 with three different multiblocks, all with an overall concentration of 14.5%, as a function of the concentration of PF multiblock copolymers. Equation 1 suggests that this plot should yield a straight line that extrapolates to c_{gel} at $G = 0$.

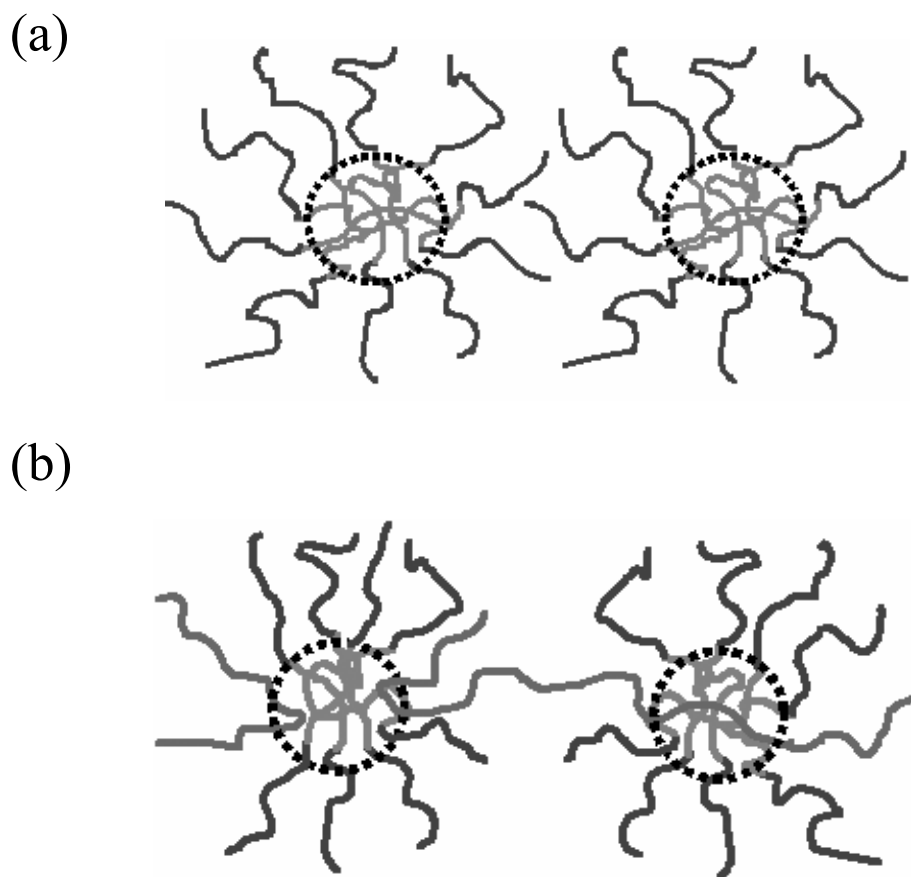


Figure 4.14 Schematic diagram for intermicellar interaction with corresponding observations in scattering and rheology measurements: (a) F127 triblock copolymer; (b) mixture of F127 and PF multiblock copolymers.